Materials Today Physics 7 (2018) 106–120

Contents lists available at ScienceDirect

Materials Today Physics

journal homepage: https://www.journals.elsevier.com/materials-today-physics

Survey of *ab initio* phonon thermal transport☆

L. Lindsay [a, *], C. Hua [b], X.L. Ruan [c], S. Lee [d, e]

[a] Materials Science and Technology Division, Oak Ridge National Laboratory, Oak Ridge, TN 37831, USA
[b] Environmental Transportation Science Division, Oak Ridge National Laboratory, Oak Ridge, TN 37831, USA
[c] School of Mechanical Engineering and the Birck Nanotechnology Center, Purdue University, West Lafayette, IN 47907-2088, USA
[d] Department of Mechanical Engineering and Materials Science, University of Pittsburgh, Pittsburgh, PA, 15261, USA
[e] Department of Physics and Astronomy, University of Pittsburgh, Pittsburgh, PA, 15261, USA

ARTICLE INFO

Article history:
Received 30 October 2018
Received in revised form
17 November 2018
Accepted 18 November 2018

Keywords:
Boltzmann equation
Density functional theory
Lattice conductivity

ABSTRACT

The coupling of lattice dynamics and phonon transport methodologies with density functional theory has become a powerful tool for calculating lattice thermal conductivity (κ) with demonstrated quantitative accuracy and applicability to a wide range of materials. More importantly, these first-principles transport methods lack empirical tuning parameters so that reliable predictions of κ behaviors in new and old materials can be formulated. Since its inception nearly a decade ago, first-principles thermal transport has vastly expanded the range of materials examined, altered our physical intuition of phonon interactions and transport behaviors, provided deeper understanding of experiments, and accelerated the design of materials for targeted thermal functionalities. Such advances are critically important for developing novel thermal management materials and strategies as heat sets challenging operating limitations on engines, microelectronics, and batteries.

This article provides a comprehensive survey of first-principles Peierls-Boltzmann thermal transport as developed in the literature over the last decade, with particular focus on more recent advances. This review will demonstrate the wide variety of calculations accessible to first-principles transport methods (including dimensionality, pressure, and defects), highlight unusual properties and predictions that have been made, and discuss some challenges and behaviors that lie beyond.

1. Introduction

Thermal management is of critical importance for advanced applications including waste heat harvesting and solid-state refrigeration with thermoelectric devices, cooling of microprocessors and memory storage devices, and thermal barrier coatings for increased Carnot efficiency. Furthermore, studying thermal processes is of fundamental scientific interest as transport limits and phonon couplings (with each other, external stimuli, and other material degrees of freedom) are not fully understood. Empowered by high-performance computing, Peierls-Boltzmann transport (PBT) combined with density functional theory (DFT) has become a powerful tool for describing phonon interactions and thermal conductivity (κ) behavior in a wide variety of materials. First-principles PBT/DFT κ calculations have demonstrated quantitative accuracy without empirical adjustable parameters and thus provide a tool for making realistic predictions of phonon interactions and transport behaviors and for interpreting related experiments. PBT/DFT methods have been applied to bulk and nanostructured materials (superlattices, two-dimensional [2D] sheets, nanowires and tubes [1D]) with a wide range of κ values (from ~0.12 W/m-K in halide perovskite nanowires [1] to 4300 W/m-K in graphene [2] at room temperature), targeting thermoelectric and thermal management applications. Advanced first-principles thermal transport calculations also provide a tool for developing novel physical insights into lattice dynamical and transport behavior.

The primary objective of this review article is to demonstrate the versatility of state-of-the-art first-principles PBT/DFT κ

☆ This manuscript has been authored by UT-Battelle, LLC under Contract No. DE-AC05-00OR22725 with the U.S. Department of Energy. The publisher, by accepting the article for publication, acknowledges that the United States Government retains a non-exclusive, paid-up, irrevocable, world-wide license to publish or reproduce the published form of this manuscript, or allow others to do so, for United States Government purposes. The Department of Energy will provide public access to these results of federally sponsored research in accordance with the DOE Public Access Plan (http://energy.gov/downloads/doe-public-access-plan).

* Corresponding author.
E-mail address: lindsaylr@ornl.gov (L. Lindsay).

https://doi.org/10.1016/j.mtphys.2018.11.008
2542-5293/

calculations by drawing attention to the variety of materials examined in the literature (Fig. 1), highlighting unusual predictions and couplings with experiment. Owing to the prodigious number of first-principles κ calculations in the literature, this review will focus primarily on calculations that involve scattering rates from quantum perturbation theory as input into the PBT/DFT formalism. Discussion of recent advances in lattice dynamics and transport toward addressing fundamental challenges presented by defects, disorder, and strong anharmonicity will be presented, as well as transport phenomena beyond the PBT/DFT description (e.g. hydrodynamic transport). The goal of this review is to provide a comprehensive resource to guide the reader to materials and applications of interest and give an overview of current trends and challenges in first-principles thermal transport calculations.

2. Phonon thermal conductivity

Fourier's law describes the linear response of an induced thermal energy current density to an applied temperature gradient across a material: $J = -\kappa \frac{\partial T}{\partial x}$. The constant of proportionality κ is the thermal conductivity of a material, a measure for how easily thermal energy can traverse it. In 1911, Einstein extended his theory of the specific heat of solids (atoms as independent oscillators) to describe κ as a random walk of thermal vibrational energy among the coupled but independent oscillators [3]. This random walk of thermal energy failed to describe the measured κ of KCl as the correlated vibrations of atoms, phonons introduced by Debye [4], actually govern thermal transport in most semiconductors and insulators.

In the context of kinetic theory, this phonon κ is given by the following equation [5,6]:

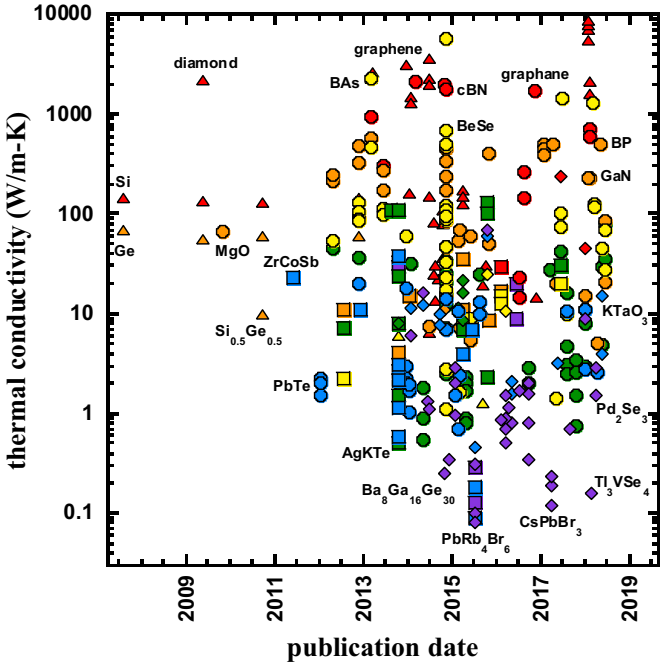

Fig. 1. PBT/DFT–calculated κ from the references given in this review. Symbol shape corresponds to the number of atoms in the formula unit of each material: one atom (triangle), two atoms (circle), three atoms (square), and four or more atoms (diamond). Color corresponds to formula unit mass (m in amu): $0 < m < 35$ (red), $35 < m < 84$ (orange), $84 < m < 150$ (yellow), $150 < m < 200$ (green), $200 < m < 400$ (blue), and $400 < m$ (purple). Note that heavier and more complex formula units (purple diamonds) tend to give lower κ. PBT/DFT, Peierls-Boltzmann transport combined with density functional theory.

$$\kappa = \sum_{\vec{q}j} C_{\vec{q}j} v^2_{\vec{q}j} \tau_{\vec{q}j} \quad (1)$$

where the sum is performed over the first Brillouin zone, $C_{\vec{q}j}$ is the volume-normalized specific heat for phonon mode with wavevector $\vec{q}$ in branch j, $v_{\vec{q}j}$ is the phonon speed, and $\tau_{\vec{q}j}$ is the phonon lifetime. Often Eq. (1) is written in terms of the phonon mean free path $l_{\vec{q}j} = \left|v_{\vec{q}j}\right| \tau_{\vec{q}j}$. Note that $v_{\vec{q}j}$ and $\tau_{\vec{q}j}$ can have directional dependence and κ is a tensor quantity as a material's response to an applied temperature gradient can vary along different crystallographic directions [7]. In practice, however, κ can be described by one (e.g. Si [7]), two (e.g. graphite [2]), or three components (e.g. SnSe [8]) for most systems.

$C_{\vec{q}j}$ and $v_{\vec{q}j}$ are determined from the phonon dispersion (frequency [ω]/wavevector relationship) of a material, which is in turn determined from the dynamical matrix constructed from harmonic interatomic force constants (IFCs) [5,6,9,10]. The real challenge in calculating κ, however, is determining the phonon lifetimes $\tau_{\vec{q}j}$ as governed by anharmonic phonon-phonon interactions, the intrinsic thermal resistance of a material. This requires calculated anharmonic IFCs that act as a perturbation to the harmonic phonon Hamiltonian in quantum perturbation theory – Fermi's golden rule. The lowest order perturbation describes three-phonon interactions and requires third-order derivatives of the interatomic potential as input [5–7].

2.1. Peierls-Boltzmann transport

The phonon lifetimes are constructed from solution of the PBT equation that describes the balance of a gas of interacting phonons driven from equilibrium by a temperature gradient $\vec{\nabla} T$ [11]:

$$\vec{v}_{\vec{q}j} \cdot \vec{\nabla} T \left(\partial n_{\vec{q}j} \big/ \partial T\right) = \partial n_{\vec{q}j} \big/ \partial t_{scatter} \quad (2)$$

The set of all possible phonon-phonon interactions are input into the right-hand side of Eq. (2). $n_{\vec{q}j}$ are the non-equilibrium phonon distributions determined by solving Eq. (2) and related to the phonon lifetimes in Eq. (1). For materials with relatively low κ (e.g. thermoelectrics or thermal barrier coatings), the relaxation time approximation (RTA) gives an appropriate solution to Eq. (2) [12,13] as Umklapp scattering (involving phonons outside the first Brillouin zone) has comparable strength to normal scattering (strictly conserves crystal momentum) [5,11]. In this case, $\tau_{\vec{q}j}$ are determined by simply summing up all the individual scattering probabilities from Fermi's golden rule. For materials with high κ (e.g. carbon-based systems [2,14]) or lower dimensionality (e.g. graphene and silicene [2,15]), full solution of Eq. (2) is necessary, for example, by self-consistent iteration [16] or variational methods [17]. Given the Peierls-Boltzmann formalism to calculate $\tau_{\vec{q}j}$ and Eq. (1) for the conductivity, the critical ingredient is an accurate description of the interatomic interactions, both harmonic and anharmonic.

2.2. Density functional theory

Various descriptions of the interatomic interactions needed to calculate harmonic (second-order derivatives of the interatomic potential) and anharmonic (typically third-order derivatives) IFCs have been developed over the years to describe stretching and bending in covalent-bonded, ionic-bonded, and van der Waals–bonded materials, including a variety of empirical

potentials [18–20] and bond-charge models [21]. However, DFT [22–27] has become the modern workhorse for thermal transport calculations. Although DFT-derived calculations of κ have a significantly higher computational cost over previous empirical potential methods, they have the advantage of applicability over a wider range of materials (structure, composition, and dimensionality) and demonstrated accuracy with no empirical tuning parameters. Thus, reliable predictions of κ behavior are possible in materials yet uncharacterized in experiments. With this said, choices must still be made regarding the various DFT flavors, including description of electronic exchange and correlations (e.g. local density approximation [LDA] and generalized gradient approximation [GGA]), representation of core and valence electrons (e.g. pseudopotentials and projector-augmented wave methods), and various convergence parameters (e.g. energy cutoffs of a plane wave basis, integration meshes in the Brillouin zone, and interaction distances). Some of these DFT aspects will be discussed later in the context of PBT/DFT calculations in the literature.

The first anharmonic calculations derived from DFT were applied to examine Raman linewidths and shifts in semiconductors [28–35]. The first coupling of PBT and DFT methodologies to calculate κ was developed in 2007 to describe isotopically purified Si and Ge [7]. This work demonstrated unprecedented quantitative accuracy over a wide temperature range with no adjustable parameters and has since inspired a plethora of *ab initio* phonon transport calculations for a variety of systems (metals, semiconductors, and insulators in one, two, and three dimensions), providing further validation, making new predictions, testing old paradigms, raising new questions, and developing understanding of measured observables. Figs. 2 and 3 compare PBT/DFT–calculated κ with measured values for BP (high κ) [36] and $CoSb_3$ and $IrSb_3$ (low κ) [37] as a function of temperature. Furthermore, PBT/DFT κ calculations have been accelerated by the availability of open-source numerical algorithms that calculate anharmonic IFCs and lattice κ [38–41]. The rest of this review will provide context and reference for many of the calculations to follow these first efforts and discuss challenges to the PBT/DFT formalism and other transport behaviors.

2.3. Testing and validation

The first publications using the PBT/DFT methodology which followed the 2007 Broido work [7] also provided strong validation for its use by comparing with measured data for diamond [14], MgO [42], and half-Heuslers [43], materials with a wide range of κ values, and for calculations over a wide temperature range. The variety of calculations was extended to involve IFCs calculated from density functional perturbation theory (reciprocal space) and DFT supercell (real space) approaches.

First-principles κ calculations can be sensitive to the approximations, cutoff, and convergence parameters used. Thus, careful consideration of DFT choices should be made depending on the desired level of quantitative accuracy. For instance, it has been demonstrated that not enforcing point group symmetries and translational invariance [13,44,45] on the calculated anharmonic IFCs of zincblende elemental and compound semiconductors can lead to lower calculated κ than when these are enforced [45]. Related to this, calculations have demonstrated that κ can vary with respect to the interaction cutoff distance (number of neighbors considered to be interacting) [45–48].

Choice of DFT flavor (LDA, GGA, or more sophisticated) can also give quantitative differences in κ calculations. Often, discrepancies are simply caused by the tendency of the LDA to overbind atoms [49], giving higher optic phonon frequencies than measured values. This can result in less calculated scattering of the heat-carrying

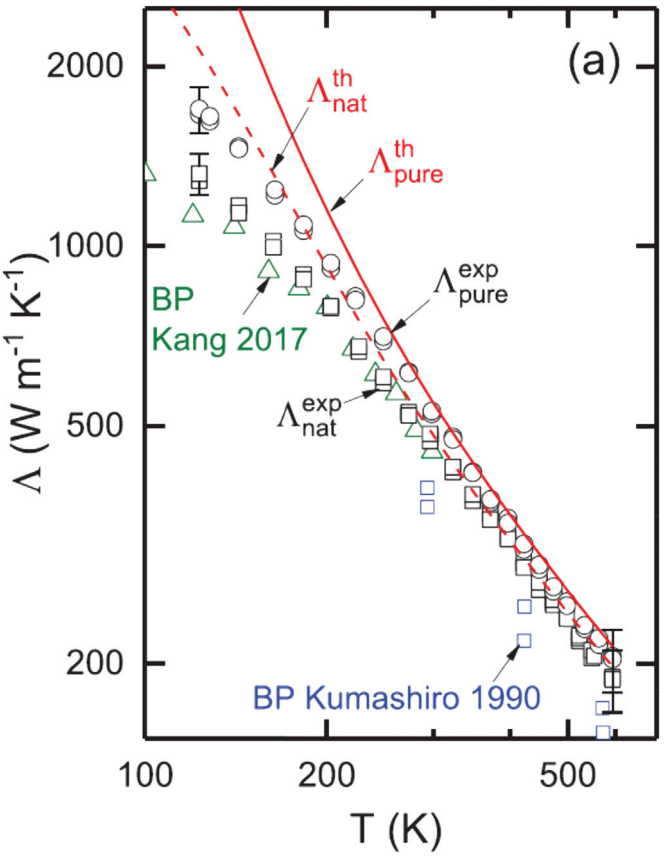

Fig. 2. Measured (symbols) and PBT/DFT–calculated (curves) thermal conductivity (Λ) of BP (black open squares and dashed red curve), isotopically pure ^{11}BP (black open circles and solid red curve), and other literature values (green triangles and blue squares) versus temperature. Reproduced from Ref. [36] with permission. PBT/DFT, Peierls-Boltzmann transport combined with density functional theory.

acoustic phonons and thus a larger κ than predicted by the GGA, which tends to do the opposite. Recent work has rigorously tested functional choice and variance among pseudopotentials in describing κ of Si [50] and graphene [51], as well as the importance of maintaining responsible convergence criteria when calculating harmonic and anharmonic IFCs. Other work has made comparisons

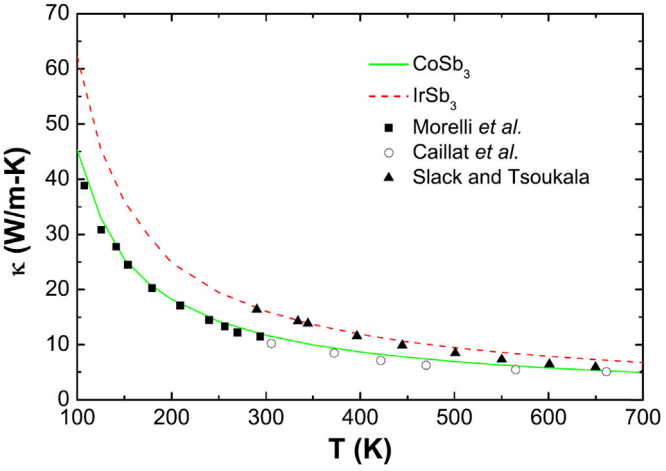

Fig. 3. Measured (symbols) and PBT/DFT–calculated (curves) κ of $CoSb_3$ (black squares, black circles, and solid green curve) and $IrSb_3$ (black triangles and dashed red curve) versus temperature. Reproduced from Ref. [37] with permission. PBT/DFT, Peierls-Boltzmann transport combined with density functional theory.

of LDA- and GGA-calculated κ in a variety of systems, including Ar [52], graphene [53], SnSe [54], $SrTiO_3$ [55], LiH and LiF [56], various metals [57], GeTe, Sb_2Te_3 and $Ge_2Sb_2Te_5$ [58], $CoSb_3$ [59], and Mg_2-IV materials [60], to name a few.

Some work has applied a more Edisonian approach to test PBT/DFT κ calculations by comparing with experimental values for a broad range of materials including zincblende and wurtzite compound III-V [40,45], IIb-VI and 1b-VII [40], and full-Heusler [61] semiconductors or by applying more sophisticated algorithms, such as high-throughput screening [62–64] to predict materials with ultralow κ, e.g. half-Heusler AgKTe [62] and $PbRb_4Br_6$ [63] with room temperature κ values of 0.51 and 0.08 W/m-K, respectively.

2.4. Four-phonon and electron-phonon coupling

Despite the incredible success of first-principles calculations based on three-phonon scattering alone, extrinsic scattering from defects (e.g. grain boundaries, vacancies, and dislocations – see Section 5) and intrinsic scattering from higher order phonon-phonon interactions and couplings to other degrees of freedom can provide significant thermal resistance in measurements. Here, we briefly highlight recent PBT/DFT efforts to include four-phonon interactions and electron-phonon coupling.

2.4.1. Four-phonon scattering

Including higher order anharmonic scattering is a challenge because of its more complex formalism [65] and demanding computational cost, despite observed discrepancies between theory and experiment, particularly at higher temperatures. For example, calculated optic phonon linewidths of many important polar materials (e.g. GaAs) were underestimated when compared to measurements, even at room temperature [29]. Furthermore, from molecular dynamics (MD) simulations (Section 7.3), another widely used method to calculate κ which includes all orders of anharmonicity, clues of the significance of fourth- and higher order anharmonicity in determining κ were elucidated by truncating the interatomic potential of argon [66].

Efforts to understand the role of four-phonon scattering in determining κ have included phase space calculations for bulk semiconductors [67], four-phonon scattering rates from simple models of carbon nanotubes [68], and qualitative assessment of quartic anharmonicity in UO_2 and CeO_2 [69]. The first rigorous perturbation theory method of four-phonon scattering rates and PBT κ was developed using empirical potentials for Ar, Si, and Ge [65].

More recently, four-phonon scattering has been incorporated into full PBT/DFT calculations of κ for diamond, Si, and BAs [70], demonstrating markedly improved agreement with measured data for diamond and Si over three-phonon-only calculations, particularly at higher temperatures. Four-phonon scattering scales as T^2, whereas three-phonon scattering scales as T; thus four-phonon scattering was found to be negligible for silicon at room temperature, but reduced κ by ~30% at 1000 K [65,70]. More surprisingly, four-phonon scattering reduced the room temperature κ of BAs by ~40% [70], more in line with recent measurements [71–73] (Fig. 4). This strong dependence on four-phonon processes in BAs is a result of the small phase space available for three-phonon scattering [74]. Similar κ suppression by four-phonon scattering of flexural phonons was found in graphene [75]. Furthermore, four-phonon scattering scales as ω^4, whereas three-phonon interactions scale as ω^2 [65,70]. Thus, four-phonon interactions are important for determining optic phonon lifetimes and linewidths over a wider range of temperature. Recently, PBT/DFT calculations of κ for strongly anharmonic materials, NaCl [76] and PbTe [77], demonstrated that both four-phonon scattering and phonon renormalization are needed for appropriate interpretation of measured data. As these

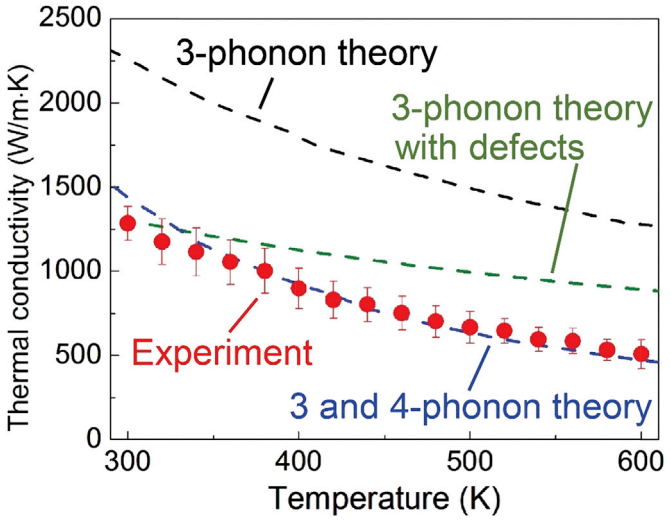

Fig. 4. Measured (red circles) and PBT/DFT–calculated κ versus temperature of BAs including three-phonon interactions only (black curve), three- and four-phonon interactions (blue curve [70]), and three-phonon and point-defect interactions (green curve). Reproduced from Ref. [71] with permission. PBT/DFT, Peierls-Boltzmann transport combined with density functional theory.

tend to give opposing effects for κ, both studies suggested that three-phonon-only calculations agreed only coincidentally with measured data for these materials.

PBT/DFT calculations have demonstrated that including higher order phonon-phonon interactions is important for accurately describing phonon lifetimes and κ particularly for (1) materials at high temperatures, (2) phonons with high frequencies, (3) materials with limited three-phonon scattering, and (4) materials with strong anharmonicity.

2.4.2. Electron-phonon coupling

Lattice distortions and vibrations can couple with electronic structure to limit electronic carrier mobility, and turning this around, electron-phonon coupling can limit lattice thermal conductivity by scattering of phonons. Recently, methods have been built to describe electron-phonon coupling from first principles [78–82] with application to thermal transport. PBT/DFT calculations coupled with first-principles description of electron-phonon coupling have been demonstrated to limit lattice thermal conductivity in heavily doped Si [83], elemental metals [57,84], and transition metal carbides [85]. PBT/DFT calculations have demonstrated that electron-phonon interactions can play an important limiting role in both phonon and electronic transport, particularly in metals or heavily doped semiconductors. Also, anomalous temperature-independent lattice κ behavior has been predicted in metals with nested Fermi surfaces (strong electron-phonon coupling) and large frequency gaps between the acoustic and optic phonons (weak phonon-phonon coupling) [85].

2.5. Temperature

Surprisingly, temperature can present a significant challenge to accurate PBT/DFT calculations of thermal transport, particularly in strongly anharmonic materials and/or materials that undergo temperature-induced phase transitions. Typical PBT/DFT calculations include the effects of temperature through the Bose-Einstein distributions of the phonons, which are built into the three-phonon scattering rates [5,7], and in the mode specific heat of Eq. (1). Such calculations, although validated by comparison with measured κ as a function of temperature for a variety of materials,

do not include the effects of thermal expansion or variations of harmonic and anharmonic IFCs with temperature. To partly address these challenges, κ calculations have been performed within the quasi-harmonic approximation [86], for which the vibrational free energy of the system is used to find structural parameters, harmonic and anharmonic IFCs for a given temperature. This method has been used to examine thermal transport in PbS, PbSe, and PbTe [87] and LiH and LiF [56]. It is to be noted that typical materials tend to expand with increasing temperature, which often gives lower frequencies. Thus, this presents a challenge for calculations that already underpredict phonon frequencies at 'zero temperature' ($T = 0$), as the GGA description of the electronic structure tends to do.

More sophisticated methods have been developed for which lattice expansion and temperature-dependent force constants are determined for subsequent κ calculations at each temperature based on small-scale MD simulations and by mapping to an effective potential [88,89], compressive sensing [90], self-consistent phonon theory [91,92], and other phonon renormalization methods including quartic anharmonicity [76,77]. These methodologies do not require that the harmonic approximation is valid at each volume/temperature considered and have demonstrated vibrational stability (no imaginary phonon modes) in materials for which $T = 0$ calculations do not. Systems studied with these approaches include PbTe [93,94], InSb [95], Bi_2Te_3 [96], $SrTiO_3$ [55], and ScF_3 [97]. Fig. 5 demonstrates the role of temperature and anharmonicity in determining the phonons of PbTe [93]. Regardless of the method, DFT determination of the IFCs is computationally expensive; thus, calculation of these at each temperature for a wide range of temperature can be a significant numerical challenge.

These sophisticated approaches for including temperature and higher order phonon interactions (Section 2.4) have demonstrated the ability to derive transport properties in materials otherwise inaccessible to PBT/DFT methods. In strongly anharmonic materials, renormalization of the phonons has demonstrated a more accurate description of the vibrational frequencies, and including higher order scattering becomes relevant for the phonon lifetimes. These methods helped elucidate the anomalous vibrational and transport behaviors of PbTe [93,94], a material near a ferroelectric instability, and predict anomalous temperature-dependent κ in ScF_3 [97], a negative thermal expansion material.

2.6. Mechanical strain

Application of pressure or strain to a material, whether bulk or 2D, can significantly alter κ and κ behavior. Early PBT/DFT calculations derived insights into the response of κ of MgO to hydrostatic pressure, with values similar to those found in the Earth's mantle, shedding light on Earth's thermal history [42]. Similar hydrostatic pressure studies have been published for Argon [52], diamond (large increase in κ with pressure) [98], and other compound materials [99,100]. Typically, κ increases with increasing pressure in bulk materials as phonon sound velocities increase and phonon coupling of heat-carrying acoustic phonons to optic modes is reduced. Opposing this, an unusual pressure response was observed with PBT/DFT calculations: κ decreasing with pressure due to increased intrinsic phonon scattering in large mass difference compounds [100], and proximity to pressure-induced phase transitions in HgTe and CuCl [101,102].

Many *ab initio* studies of the effects of the application of strain on κ in 2D materials have also demonstrated some unusual κ behaviors. Isotropic strain was predicted to change κ minimally for small strains, ~1% in samples with size ~10 μm [53,103]. Non-monotonic κ response, first increasing κ for moderate strain and then decreasing κ with increasing strain, was predicted for graphene's cousins, (silicene, germanene, and stanene) [15,104], and multilayer graphene and BN [105]. The interplay of size and strain was examined in graphene and MoS_2 [103,106].

Pressure and strain have been shown to give a variety of different κ behaviors, all linked to induced changes in the phonon dispersions as the structure is manipulated. PBT/DFT calculations have demonstrated that softening transverse acoustic modes enhances scattering resistance [102], whereas hardening optic modes gives reduced resistance [100]. In some cases, an interplay of these features, as well as with varying phonon velocities, can give rise to

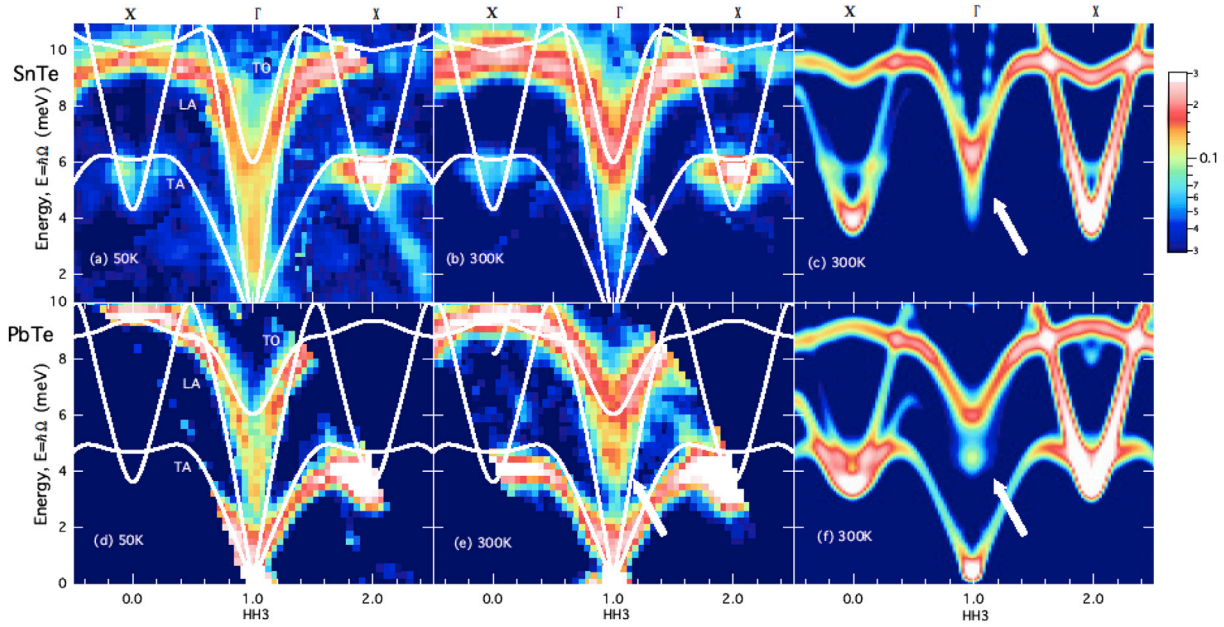

Fig. 5. Measured imaginary dynamical susceptibilities for SnTe (a, b) and PbTe (d, e) at T = 50 K and T = 300 K, respectively, compared with first-principles calculations of the same at T = 300 K (c, SnTe; f, PbTe), demonstrating anomalous behavior of the zone center transverse optic mode. Reproduced from Ref. [93] with permission.

non-monotonic κ behavior as a function of strain and pressure [15,104].

3. High κ and low κ materials for applications

A key utility of the PBT/DFT methods described previously is to predict and design novel thermal functionalities for new and known materials and to develop deeper physical insights into the thermal processes that drive them. This section will highlight application of PBT/DFT methods to probe high and low κ regimes toward thermal management applications.

3.1. Thermal management materials (high κ)

Carbon-based materials have long been known to have the highest κ of all systems: diamond, graphite, and graphene. Guided by the physical properties of these materials, four basic empirical rules were developed to understand the origins of high κ: (1) simple crystal structure, (2) strong interatomic bonding, (3) light atomic mass, and (4) low anharmonicity [107,108]. Strong bonding and light mass combine to give stiffer phonons with larger velocities to better carry heat, and low anharmonicity gives increased phonon lifetimes. In the search for new high κ materials, PBT/DFT calculations have tested and augmented these rules in terms of the number of phonon-phonon scatterings available given conservation of energy and momentum conditions (scattering phase space). This phase space is governed by features of the phonon dispersions, and it was found that high κ can also occur in materials with (1) a large gap between heat-carrying acoustic phonons and optic modes [109,110], (2) acoustic branches tightly grouped together [74,111], and (3) small bandwidth of the optical branches [46,112]. Recent first-principles calculations have been used to further probe lattice κ and guide experimental efforts to attain high κ in materials including GaN [109,113–115], SiC [116,117], diamond and BN variants [118], and BP [36].

To further highlight the predictive utility of PBT/DFT κ calculations and to tie together many of the topics discussed in this survey, the various efforts to examine thermal transport in zincblende BAs are discussed here. Given the empirical rules described previously and a simple model, Slack predicted BAs to have κ~200 W/m-K [107]. However, a later PBT/DFT calculation predicted a room temperature κ value ~2200 W/m-K [74], nearly that of the best bulk conductor diamond, despite the BAs average mass being nearly 3.5 times larger. In that work, this discrepancy was attributed to a large frequency gap between acoustic and optic phonons and bunching together of the acoustic branches, severely limiting the phonon scattering phase space. However, these arguments were based on features of the phonon dispersion which were not yet measured; only frequency measurements of zone center Raman-active optic modes [119] gave some validation of the calculated dispersion. Subsequently, BAs crystals were synthesized and characterized (Raman [119,120], X-rays [121], and κ [122–124]) with measured κ values ~200–350 W/m-K, more in line with Slack's arguments and prediction from decades earlier [107]. X-ray scattering measurements verified the predicted acoustic/optic frequency gap and bunching of the acoustic phonons [121]; however, phonon linewidths/lifetimes were not reported. The discrepancy of measured and predicted κ was attributed to extrinsic crystal defects, including grain boundaries, As vacancies [125], and paired B and As antisite defects [126]. Subsequent PBT/DFT calculations including four-phonon scattering predicted lower κ for BAs: ~1400 W/m-K [70] and ~1250 W/m-K [73] at room temperature. Very recent synthesis and characterization efforts from three separate research groups have demonstrated growth of relatively large (~mm), high-quality BAs crystals with room temperature κ values greater than 1000 W/m-K [71–73]. The largest κ value achieved in measurement at room temperature was 1300 W/m-K [71], in reasonable agreement with predictions including four-phonon processes over a wide temperature range as shown in Fig. 4.

3.2. Thermoelectric materials (low κ)

On the opposite κ spectrum to BAs, low κ materials are of extreme importance for thermal insulation, barrier coatings for improved Carnot efficiency, and for waste heat harvesting and solid-state refrigeration using thermoelectrics. Low κ materials challenge PBT/DFT calculations as these often have soft vibrational modes, many scattering channels to compute, strong anharmonicity, and questionable relevance of the phonon picture. Nonetheless, many interesting insights have been elucidated from PBT/DFT κ calculations in low κ materials, some of the earliest work done with relation to Si/Ge alloys and nanostructures [127–129]. Observation and calculation of a soft transverse optical branch governed by a ferroelectric instability in the prototypical thermoelectric material PbTe [93,130,131] spurned numerous PBT/DFT calculations in lead chalcogenide–derived systems [12,77,87,94,132] including intrinsically localized mode behavior in PbSe [133]. Other model thermoelectric materials for which first-principles calculations have shed light on thermal transport behavior include Bi_2Te_3 [96], Mg_2Si/Sn alloys [13], SnSe [8,54,134], skutterudite $CoSb_3$ and filler modes [37,59,135,136], and rattling atoms in clathrate materials [137–139]. Empowered by predictive PBT/DFT thermal transport calculations, new materials with enhanced electronic properties and ever lower κ values are explored; example materials and room temperature κ values include ScN (20 W/m-K) [140], 2D IV-VI chalcogenides (3–16 W/m-K) [141], NaI (1.64 W/m-K) [142], different HgTe phases (0.6–10.5 W/m-K) [143], CaF_2 (8.6 W/m-K) [144], Ca_3Si_4 (3.2 W/m-K) [145], full Heuslers (0.5–1.5 W/m-K) [61], $TlBiSe_2$ (0.85 W/m-K) [146], skutterudites including $YbFe_4Sb_{12}$ (0.34 W/m-K) [136], $SnFe_4Sb_{12}$ (0.7 W/m-K) [147], Fe_2Ge_3 (1.8 W/m-K) [148], $FeSb_3$ (1.14 W/m-K) [149], BiCuOTe (0.8 W/m-K) [150], $BaCd_2Sb_2$ (0.95 W/m-K) [151], perovskites $KTaO_3$ (15 W/m-K) and $PbTiO_3$ (4 W/m-K) [152], and halide perovskite nanowires (0.12–0.24 W/m-K) [1].

As the acoustic phonon contributions to κ are suppressed in highly anharmonic low κ materials, optic phonons can provide non-negligible contributions to the overall κ despite their typically smaller velocities and lifetimes. This unusual behavior has been observed in Ga_2O_3 [153], prototypical phase change material $Ge_2Sb_2Te_5$ [154], and mass-functionalized graphene [155].

PBT/DFT calculations have probed the lower limit to κ in crystalline materials and have provided physical insights into a myriad of vibrational features that enhance thermal resistance in materials with simple or complex structures. For example, resonant bonding in PbTe, SnTe, and other materials was demonstrated to give long-ranged interactions and enhanced scattering [46]. Acoustic-optic hybridization and avoided branch crossings have also been shown to give enhanced resistance in materials [136,148]. Similarly, low-frequency optic branches in materials near phase transitions [93,130,131,149,152] or from rattling modes in skutterudites [147] have been associated with enhanced phonon scattering and low κ.

4. Nanostructures

Nanostructures such as superlattices and nanowires are known to suppress κ for enhanced thermoelectric performance via scattering of phonons from interfaces and boundaries; however, ultrahigh κ values can also be achieved in 1D and 2D materials as phonon behaviors and scatterings are significantly altered from

their bulk behaviors. Here, we highlight first-principles PBT/DFT calculations of κ in lower dimensional and nanostructured materials.

4.1. Lower dimensional materials

A striking success of the PBT/DFT formalism is its applicability to lower dimensional materials. These methods have validated previous predictions based on empirical models [156,157] of the transport behavior in the prototypical 2D material graphene with its ultrahigh measured [158–161] and predicted [2,53] κ and have elucidated other possible transport mechanisms (e.g. ballistic and hydrodynamic transport [162,163] as discussed in Section 7.2). Despite reduced number of integrations required to describe κ in 2D materials, these systems present particular challenges not encountered in bulk, including a quadratic acoustic flexural branch (often labeled ZA) [164], ill-defined material thickness (experiment and theory), which is required to compare 2D κ to that in bulk materials [165], questionable convergence/divergence with infinite system size [15,53,103,166,167], validity of the relaxation time approximation [53,162,163], and large number of integration points required to adequately describe phonons and transport [15,103]. Regardless of these challenges, as 2D materials (and their bulk layered counterparts) have emerged as potential candidates for various novel technologies, so too have PBT/DFT κ calculations for them, including for MoS_2 [106,168,169], WSe_2 and WTe_2 [170,171], black and blue phosphorene [167,172,173], graphene's cousins (silicene, germanene, stanene and graphane [15,104,155,163,174]), hexagonal BN [105,163], SnSe [8,54,134], Pd_2Se_3 [175], InSe [176,177], MXenes [178,179], and borophene and borophane [180–182], to name a few. *Ab initio* methods have also been applied to examine thermal transport in a few 1D systems, although with the challenges described previously for 2D systems exaggerated. To date, first-principles PBT/DFT calculations include diameter dependence of κ in single-walled carbon nanotubes [183], comparing bulk and 1D polyethylene [184], $Ta_2Pd_3Se_8$ nanowires [185], and Ba_3N chains [186].

PBT/DFT κ calculations in lower dimensional materials have elucidated the roles of structure, bonding, and dimensionality in determining transport behavior. For example, calculations give new phonon-phonon scattering selection rules based on reflection symmetries [53] or quantum phonon chirality [186,187]. Buckling of materials [15,104,155,167,172–174] and coupling with other layers or a substrate [156] breaks these scattering rules, giving stronger interactions and lower κ.

4.2. Nanostructured materials

The PBT/DFT formalism has also been used to describe κ of different thin film, nanowire, and superlattice systems. The combination of materials in short-period superlattices gives coherent wave interference effects (alters their phonon dispersions) [188] and provides scattering interfaces that can limit phonon transport, thus enhancing the thermoelectric figure of merit. Vibrational properties and κ of Si/Ge superlattices were calculated [129,189–192], elucidating an interesting enhancement to κ in the short-period limit and the role of material intermixing at the interfaces. In a high-profile publication, calculations of AlAs/GaAs superlattices accompanied experimental demonstration of coherent acoustic phonon transport across superlattice interfaces [193,194]. A more recent theoretical/experimental collaboration has examined tailored κ in InAs/GaAs superlattices [195]. PBT/DFT methods have also been applied to examine coherent effects in thin films and porous structures, including diffusive and ballistic phonon conductivity in Si porous films [196,197] and mean free path distributions in Si with nanopatterned heating array experiments [198]. Some early nanowire κ calculations iteratively solved the PBT including phonon distributions that were spatially dependent for Mg_2Si/Sn alloys [13], diamond, and Si [199].

5. Defects and disorder

5.1. Isotopes

The first PBT/DFT calculations for κ of Si and Ge showed remarkable agreement with measurements but were only compared with isotopically enriched samples of very high quality in which intrinsic three-phonon scattering was presumably the dominant thermal resistance. The following work, calculating κ for Si, Ge, and diamond [14], demonstrated that including phonon scattering from isotopic mass variations via quantum perturbation theory [200] provides equally good agreement with measured data, without adjustable parameters, thus extending the applicability of this method. Subsequent work has since demonstrated that isotopes can play an important role in scattering phonons in materials for which the intrinsic three-phonon scattering is weak, for example, at lower temperatures or in compound materials with a large mass mismatch of the constituent atoms [201]. One notable prediction was a 65% enhancement to the room temperature κ of GaN with isotopic purification of the heavy Ga atoms [109]; this is compared to the largest measured room temperature isotope effects for diamond and graphene ~50% [202] and ~60% [161], respectively. PBT/DFT calculations predict only a modest ~10–15% RT κ enhancement for isotopically purified graphene [2,53,103], a notable and unresolved discrepancy, although still within the measured error bars.

5.2. Extrinsic defects

First-principles calculations of κ are complicated further when comparing with measured κ in materials with significant phonon-defect interactions with, for example, vacancies, surfaces, and dislocations. Often, these phonon-defect scattering mechanisms are described by formulas simplified from perturbation methods or from empirical observations and are coupled to intrinsic phonon-phonon scattering from PBT/DFT calculations. Here, we highlight recent advances coupling PBT/DFT with Green's function methods to provide fully *ab initio* calculations of κ in materials with defects. Phonon-vacancy scattering from DFT Green's function methods have been found to be nearly an order of magnitude stronger in diamond [203], BAs [125], graphene [204], and InN [205] than that from previous empirical methods. Structural relaxation and IFC variance play a critical role toward scattering phonons, beyond simple mass and first-order perturbation theory approximations. Similar effects were also found for isotope clusters in graphene [206] and substitutional atoms in SiC [116], graphene [204], GaN [114], FeSi [207], InN [205], and antisite defects in BAs [126]. This methodology was even applied to examine phonon-dislocation scattering and thermal transport in Si [208] and to describe conductance across interfaces in Si/Ge (including only mass variations) [128,129] and gold/alkane interfaces [209], as well as electron-phonon couplings in metal/semiconductor interfaces TiS_2/Si and $CoSi_2/Si$ (including force and mass variations) [210,211].

5.3. Alloy disorder

As discussed with defects previously, variation of masses and IFCs from those given by the perfect crystal structure can be a very strong scattering mechanism for phonons. Thus, another challenge

for PBT/DFT κ calculations is describing strongly disordered materials, such as alloys. The first such calculations used the virtual crystal approximation (VCA) to describe thermal transport in Si_xGe_{1-x} [127], $PbTe_xSe_{1-x}$ [12], and $Mg_2Si_xSn_{1-x}$ [13] alloys for thermoelectric applications. The VCA averages the properties of the end components (e.g. harmonic and anharmonic IFCs, lattice constants, etc.) based on the concentration of each. On top of this, the mass variance of the alloy system is considered within quantum perturbation theory, similar to isotope mass variance [12,13,127,200]. This approach has demonstrated reasonable agreement with κ and phonon lifetime measurements despite neglecting phonon scattering from variations in the IFCs. Other VCA alloy calculations have been applied to κ of other PbTe-based alloys [212]; $Mg_xCd_{1-x}O$ [213]; 2D alloys of InSe, GaSe, and GaS [177]; and Bi-Sb alloys [47], with other approximations in the thermoelectric $Ge_xMn_{1-x}Te$ [214], and with embedded particles in Si/Ge alloys [215]. Force constant variation was shown to be significant for phonon-defect calculations and likely plays an important role in alloys. This was demonstrated by recent PBT/DFT κ calculations using quasi-random supercells and Green's function methods for $In_{1-x}Ga_xAs$ alloys [216] (Fig. 6).

Mass variance scattering from perturbative methods coupled with PBT/DFT calculations have successfully described κ when including isotopic disorder [14,109] and, in some cases including, alloy disorder using the VCA [12,13,127]. However, coupling of PBT/DFT with Green's function calculations for materials with point defects, dislocations, and interfaces have demonstrated the importance of including force constant disorder and the breakdown of perturbative models for describing phonon scattering and transport.

6. Experimental probes

Various methods are available for probing structural, vibrational, and thermal properties of materials. This section briefly highlights some PBT/DFT calculations that have been coupled with such experiments to develop deeper physical insights into phonon behaviors.

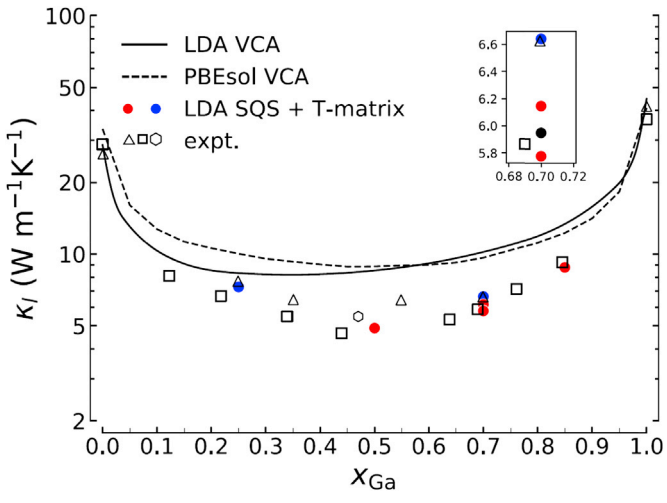

Fig. 6. Measured (hollow black symbols) and calculated thermal conductivity (κ_l) of $In_{1-x}Ga_xAs$ alloys as a function of x at T = 300 K. PBT/DFT calculations are given by curves (using the VCA) and filled circles (using Green's functions and special quasi-random supercells [red, 128 atoms; blue, 250 atoms]). Note that curves only consider mass disorder scattering, whereas filled circles consider both mass and force constant disorder. Reproduced from Ref. [216] with permission. LDA, local density approximation; PBEsol: Perdew-Burke-Ernzerhof-solid; PBT/DFT, Peierls-Boltzmann transport combined with density functional theory; SQS: special quasi-random supercells; VCA, virtual crystal approximation.

6.1. Raman, X-rays, and neutrons

Some of the first *ab initio* anharmonic phonon calculations were designed to understand temperature, pressure, and isotope dependence of phonon frequency shifts and linewidths (inverse of phonon lifetimes) of Raman modes in semiconductor crystals (e.g. Si and GaAs) and later in more exotic systems (e.g. BN, graphene, Bi_2S_3, MoS_2, and $CH_3NH_3PbI_3$) [28–35,217–219]. Recently, measured Raman linewidths in isotopically modified BN compared favorably with first-principles calculations, which provided an upper bound to the isotopically pure lifetime limit [35]. Raman linewidth measurements were also used to validate phonon lifetime predictions for Tl_3VSe_4 [220].

For 2D materials, Raman thermometry has become an important laser-based spectroscopic technique for extracting thermal conductivity values. This non-destructive technique determines κ from the laser power absorbed in the sample and changes in measured Raman-active modes [158–161]. PBT/DFT calculations have been compared with Raman thermometry measurements of κ for graphene [53,103] and used in conjunction with these experiments to provide insights for MoS_2 [221].

Inelastic neutron scattering (INS) and inelastic X-ray scattering (IXS) techniques are also valuable tools for probing phonon frequencies, optic and acoustic, throughout the entire Brillouin zone of a material. Depending on instrumental resolution, these methods can also give information of phonon lifetimes, provided these are sufficiently small (large linewidths) as in typical thermoelectrics and other low κ materials. INS and PBT/DFT calculations have been coupled to understand the role of anharmonicity in determining phonon lifetimes and κ in UO_2 [222], spectral functions in PbTe [93], and spectral weight in the density of states in CuCl [102]. IXS and PBT/DFT have also been coupled to understand the low κ behavior in $PbTe_{1-x}Se_x$ alloys [132] and to validate phonon dispersion features critical to the high κ prediction in BAs [121], as discussed previously.

6.2. Thermal spectroscopies

More recently, ultrafast laser spectroscopies have been developed to measure the thermal conductivity of various material systems [223–229]. Unlike most traditional thermal measurement techniques [230], these optical methods can be used to probe microscopic features of phonons in solids through observations of quasiballistic transport behavior, providing mode-dependent information and more restrictive tests of PBT/DFT calculations. Quasiballistic thermal transport occurs if a temperature gradient exists over a length scale comparable to the phonon mean free paths (MFPs) [231,232]. In experiments, measured κ reduction with varying length scale of the imposed temperature gradient is due to quasiballistic phonon thermal transport. This behavior has been reported in numerous experiments using transient grating spectroscopy [233,234], thermoreflectance methods [198,235–240], soft X-ray diffraction [241,242], and lithographically patterned metallic heaters [243,244]. These quasiballistic transport observations have been used to reconstruct the MFP distribution of phonons in various materials [198,243,245,246]. Recent thermal measurements in single-crystal BAs using thermoreflectance techniques not only confirmed the ultrahigh thermal conductivity of BAs [71–73] but also revealed the phonon MFP spectra of BAs through a series of observations of quasiballistic thermal transport, agreeing well with the PBT/DFT–calculated MFP spectra [71]. These measurements further validated the PBT/DFT predictions from a more rigorous microscopic perspective. Besides phonon MFP spectra, the experimental observation of quasiballistic thermal transport also reveals insights of the microscopic processes of

phonon transport across grain boundaries and interfaces when combined with *ab initio* modeling [234,240] (Fig. 7). For example, a metrology to extract phonon transmission coefficients at solid interfaces using first-principles phonon transport modeling and time-domain thermoreflectance (TDTR) experiments was recently developed [240]. In another study, phonon wavelength–dependent specularity parameters were extracted from macroscopic thermal conductivity measurements in a transient thermal grating experiment by interpretation of the measured observables with an *ab initio* description of phonon transport [234]. Ultrafast laser-based spectroscopies combined with PBT/DFT calculations have been demonstrated as a powerful tool to study the intrinsic properties of phonons in solids and microscopic processes near different structural features, including interfaces.

7. Beyond Peierls-Boltzmann transport

7.1. Limitations of PBT/DFT

Most of the work highlighted in this survey has used a linearized form of the homogenous, steady-state Peierls-Boltzmann equation (Eq. (2)), typically with phonon-phonon interactions only to lowest order in perturbation theory (Sections 2.4 and 2.5 for exceptions). In this case, phonons are assumed to be well-defined quasiparticles that do not interact too strongly and whose distributions respond linearly to a temperature gradient [5–7,11,247]. Furthermore, the material that supports them has no spatial (besides a small and linear temperature gradient) or temporal variations. Thus, this form of the PBT does not consider the effects of temperature profiles that oscillate in time or vary on the surface of a material, similar to many of the laser-based thermal spectroscopies discussed previously. Relevance of these features depends on the spatial and temporal scales for temperature variations compared with the vibrational dynamics. Also, the PBT method does not account for variations in the phonon distributions near a surface or interface of a material. Although more challenging to solve, a more general form of the PBT including spatial and temporal variation has been used to describe thermal transport in bulk diamond, Si and MgO [248], nanoribbons [249], and nanowires [13,199].

Application of PBT methods also becomes questionable for materials with extreme disorder (alloys lacking periodicity) or crystals with strong anharmonicity (phonon MFPs on the order of the lattice spacings), and the description of the normal mode vibrations becomes blurred. Atomistic simulations have demonstrated that vibrations in amorphous materials can be localized (locons), phonon-like (propagons), or neither (diffusons) [250–252]. Even in crystalline materials, higher manganese silicide ladder structures [253] and Tl_3VSe_4 [220], comparison of PBT/DFT calculations with measurements of κ, suggest that vibrational thermal energy may be carried by both phonons and 'hopping' of instantaneously localized vibrational thermal energy.

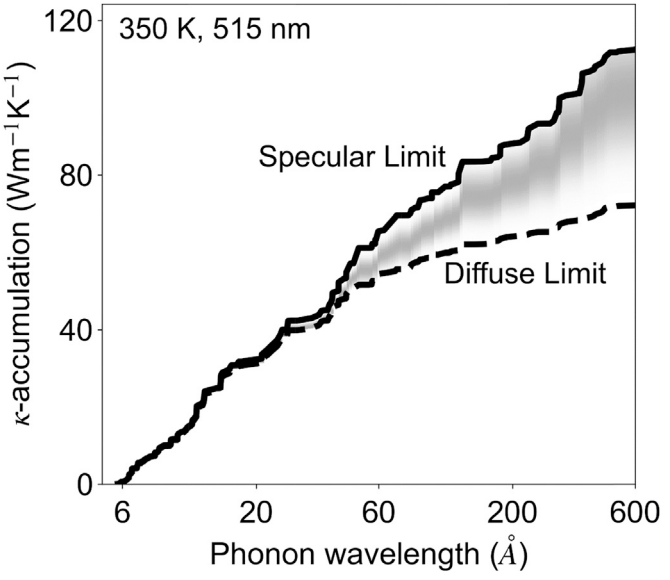

Fig. 7. Calculated thermal conductivity accumulation (κ-accumulation) versus phonon wavelength for a Si membrane with thickness of 515 nm at 350 K. The solid (dashed) black curve represents the specular (diffuse) scattering limit, and the gray region is calculated using specularity parameters extracted from interpreting macroscopic thermal conductivity measurements in a transient grating experiment with an *ab initio* description of phonon transport. Reproduced from Ref. [234] with permission.

7.2. Hydrodynamic phonon transport

When normal (N) scattering is much stronger than Umklapp (U) scattering, and thus most scattering processes conserve the total momentum of the flowing phonon distribution, hydrodynamic phonon transport can occur. This phonon transport is similar to fluid flow in that the phonon scattering conserves the overall momentum similar to intermolecular scattering, hence the term 'hydrodynamic'. Hydrodynamic phonon transport was an active research topic in the 1960s and 1970s, with theoretical predictions [254–257] followed by later experimental confirmation [258–261]. These studies verified the quantum theory of lattice dynamics by demonstrating dissimilar effects of N- and U-scattering processes on phonon transport and are thus of scientific significance. However, hydrodynamic phonon transport was only observed at extremely low temperatures (<20 K) and thus not of interest for practical applications.

Recent advances in *ab initio* simulation of phonon transport have brought renewed attention to hydrodynamic phonon transport. PBT/DFT scattering rate calculations demonstrate that in some high κ materials such as diamond [14], graphene [2,53], and graphite [2], N-scattering is much stronger than U-scattering, even at room temperature. As briefly mentioned in Section 2.1, both N- and U-scatterings play important roles in determining the full solution of the PBT, U being strictly resistive and N redistributing phonons. Both are required to give agreement with measured data, particularly for high κ materials. Strong N-scattering is the basis of recent predictions of hydrodynamic phonon transport in suspended graphene using the *ab initio* phonon calculation framework [162,163]. Full solutions of the PBT show that phonons exhibit a collective motion with the same drift velocity. Hydrodynamic phonon transport was also predicted in single-walled carbon nanotubes [262] and graphite [263]. These first-principles phonon calculations for graphitic materials predict that the hydrodynamic regime dominates over ballistic and diffusive regimes in a wide range of temperature, 50–150 K, depending on the sample size. Also, even at room temperature, it was shown that the hydrodynamic regime cannot be neglected, but all three regimes coexist [162,163,263,264] (Fig. 8).

The description of hydrodynamic phonon transport requires a full solution of the PBT in both reciprocal and real spaces. The real-space component is required in the hydrodynamic regime as the main thermal resistance is due to a viscous damping, momentum transfer through many N-scattering processes to boundary walls, and subsequent destruction of momentum by diffuse boundary scattering [264]. The PBT in Eq. (2) assumes that the MFPs of phonons limited by U-scattering are much smaller than the sample size and thus the temperature gradient and phonon distribution function are homogenous in the material. Solving the PBT in both

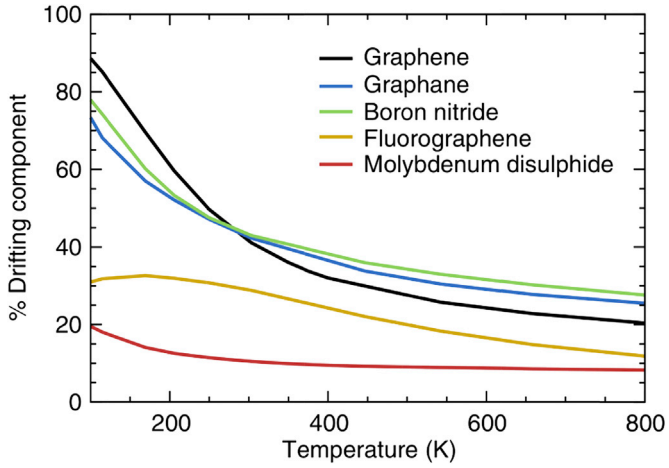

Fig. 8. The drifting (hydrodynamic) component of phonon flow in various two-dimensional materials versus temperature, demonstrating significant hydrodynamic phonon transport in graphene, graphane, and boron nitride. Reproduced from Ref. [163] with permission.

real and reciprocal spaces can be a challenging task as the PBT is an integro-differential equation with many dimensions. Recently, two *ab initio* approaches were developed. First, the concept of the 'relaxon', an eigenstate of the symmetrized scattering operator, was introduced [265]. In this approach, the PBT is recast in terms of distribution functions of relaxons. An advantage of introducing the relaxon is that phonon transport can be described by a simple kinetic theory of relaxons with well-defined quasiparticle MFPs. Second, a Monte Carlo (MC) method was developed to solve the PBT with a full scattering matrix [249,264]. Previously, the MC method was used to solve the PBT with a single-mode RTA to study quasi-ballistic phonon transport [266,267]. For solving the PBT with a full scattering matrix, a specific scattering channel among many scattering channels is stochastically chosen. An advantage of the MC method is that sample distribution functions of ballistic and scattered particles can be found separately, and therefore, the different contributions from ballistic, hydrodynamic, and diffusive regimes to the actual phonon transport can be quantitatively elucidated [268]. This is particularly useful for the case in which all three regimes coexist, which commonly occurs in high κ materials at room temperature.

Ab initio calculations have demonstrated the importance and complex interplay of N- and U-scattering in determining phonon hydrodynamic behavior, including second sound. These have predicted the temporal and spatial scales required to observe hydrodynamic behavior for a number of materials (including graphene [162,163], graphite [263], and carbon nanotubes [262]) at relatively high temperature and have given deeper insights into phonon transport behavior in high κ materials. Experimental observation of hydrodynamic behavior in the predicted spatial and temporal scales would demonstrate the predictive power of these extended first-principles frameworks.

7.3. First principles–enabled MD

MD simulations are another powerful tool for calculating κ, particularly for applications in which PBT/DFT calculations are not effective. For instance, *ab initio* MD was combined with phonon normal mode analysis and the PBT to predict κ of MgO at high temperature and pressure [269]. First-principles MD simulations have also used the transient response of the system to predict κ of nanostructures [270] and given insights into large atomic displacements and transport in Cu_2Se [271]. However, *ab initio* MD can handle only small simulation domains due to the large computational expense; thus, it is most suitable for small nanostructures or bulk materials at high temperatures. More typically, MD simulations use empirical potentials that are often not available for materials of interest. Alternatively, first-principles data sets (including cohesive energies and bond lengths, for example) have been used with other experimental data to develop potentials for materials such as silicon [272] and carbon [19]. However, most empirical potentials were not developed with thermal transport in mind. For thermal transport, the potentials need to capture essential harmonic and anharmonic phonon properties at the temperatures of interest. Recently, progress toward this goal has been made by using first-principles energy surface data corresponding to the atomic displacements at relevant temperatures [273], adjusting potential parameters to fit phonon dispersions [274], and introducing third-order force constants and genetic algorithms in the fitting process [275].

8. Concluding remarks

This article has provided a review of the literature related to PBT/DFT methods and applications, highlighting the wide variety of materials that have been examined, some interesting predictions, and recent methodological developments. The PBT/DFT provides a capability to reliably predict κ of a variety of materials (from 1D to bulk) and systems (e.g. superlattices and alloys) under a variety of conditions (e.g. temperature and pressure). Since its inception just over a decade ago, PBT/DFT has been benchmarked against measured κ data for a number of materials demonstrating general quantitative accuracy without adjustable empirical parameters. Application of PBT/DFT to different materials has resulted in new physical insights into the nature of phonon scattering and thermal transport and some exciting predictions. Recent extensions of the PBT/DFT formalism include phonon interactions with defects and higher order anharmonic processes, generally extending its applicability.

As access to computational power and numerical software packages increases, application of the PBT/DFT formalism to novel material systems and further expansion of its predictive power are inevitable. Green's function algorithms and supercell zone-folding techniques will likely be further developed for modeling the variety of phonon-defect interactions in 'real' materials for coupling with PBT/DFT transport, including defect dynamics. Phonon renormalization and higher order phonon interactions will become the norm rather than the state of the art. Advances in the first-principles description of electron-phonon interactions and coupling with PBT/DFT will pave the way for phonon coupling and transport descriptions (ballistic, diffusive, hydrodynamic, etc.) with other degrees of freedom, including magnons and other vibrational channels. This is an exciting time to develop enhanced theoretical and numerical descriptions of thermal transport in solids.

Acknowledgments

L.L. acknowledges support from the U. S. Department of Energy, Office of Science, Basic Energy Sciences, Materials Sciences and Engineering Division. C.H. acknowledges support from the Laboratory Directed Research and Development Program of Oak Ridge National Laboratory, managed by UT-Battelle, LLC, for the U.S. Department of Energy. X.L.R. acknowledges partial support from the National Science Foundation (Award No. 1150948) and Defense Advanced Research Projects Agency (Award No. HR0011-15-2-0037). S.L. acknowledges support from the National Science Foundation (Award No. 1705756 and 1709307).

References

[1] W. Lee, H. Li, A.B. Wong, D. Zhang, M. Lai, Y. Yu, Q. Kong, E. Lin, J.J. Urban, J.C. Grossman, P. Yang, Ultralow thermal conductivity in all-inorganic halide perovskites, Proc. Natl. Acad. Sci. 114 (2017) 8693.

[2] G. Fugallo, A. Cepellotti, L. Paulatto, M. Lazzeri, N. Marzari, F. Mauri, Thermal conductivity of graphene and graphite: collective excitations and mean free paths, Nano Lett. 14 (2014) 6109–6114.

[3] A. Einstein, Elementary observations on thermal molecular motion in solids, Ann. Phys. 340 (1911) 679–694.

[4] P. Debye, On the theory of specific heats, Ann. Phys. 344 (1912) 789–839.

[5] J.M. Ziman, Electrons and Phonons: the Theory of Transport Phenomena in Solids, Oxford University Press, London, 1960.

[6] G.P. Srivastava, The Physics of Phonons, Taylor & Francis Group, New York, 1990.

[7] D.A. Broido, M. Malorney, G. Birner, N. Mingo, D.A. Stewart, Intrinsic lattice thermal conductivity of semiconductors from first principles, Appl. Phys. Lett. 91 (2007) 231922.

[8] J. Carrete, N. Mingo, S. Curtarolo, Low thermal conductivity and triaxial phononic anisotropy of SnSe, Appl. Phys. Lett. 105 (2014) 101907.

[9] N.W. Ashcroft, N.D. Mermin, Solid State Physics, Thomson Learning, Inc., Philadelphia, 1976.

[10] S. Baroni, S. de Gironcoli, A. Dal Corso, P. Giannozzi, Phonons and related crystal properties from density-functional perturbation theory, Rev. Mod. Phys. 73 (2001) 515–562.

[11] R.E. Peierls, On the kinetic theory of thermal conduction in crystals, Ann. Phys. 3 (1929) 1055–1100.

[12] Z. Tian, J. Garg, K. Esfarjani, T. Shiga, J. Shiomi, G. Chen, Phonon conduction in PbSe, PbTe, and $PbTe_{1-x}Se_x$ from first-principles calculations, Phys. Rev. B 85 (2012) 184303.

[13] W. Li, L. Lindsay, D.A. Broido, D.A. Stewart, N. Mingo, Thermal conductivity of bulk and nanowire $Mg_2Si_xSn_{1-x}$ alloys from first principles, Phys. Rev. B 86 (2012) 174307.

[14] A. Ward, D.A. Broido, D.A. Stewart, G. Deinzer, Ab initio theory of the lattice thermal conductivity in diamond, Phys. Rev. B 80 (2009) 125203–125210.

[15] Y.D. Kuang, L. Lindsay, S.Q. Shi, G.P. Zheng, Tensile strains give rise to strong size effects for thermal conductivities of silicene, germanene and stanene, Nanoscale 8 (2016) 3760–3767.

[16] M. Omini, A. Sparavigna, An iterative approach to the phonon Boltzmann equation in the theory of thermal conductivity, Phys. B Condens. Matter 212 (1995) 101–111.

[17] G. Fugallo, M. Lazzeri, L. Paulatto, F. Mauri, Ab initio variational approach for evaluating lattice thermal conductivity, Phys. Rev. B 88 (2013) 045430–045438.

[18] F.H. Stillinger, T.A. Weber, Computer simulation of local order in condensed phases of silicon, Phys. Rev. B 31 (1985) 5262.

[19] J. Tersoff, Empirical interatomic potential for carbon with applications to amorphous carbon, Phys. Rev. Lett. 61 (1988) 2879.

[20] D.W. Brenner, Empirical potential for hydrocarbons for use in simulating the chemical vapor deposition of diamond films, Phys. Rev. B 42 (1990) 9458.

[21] W. Weber, Adiabatic bond charge model for the phonons in diamond, Si, Ge, and α, Phys. Rev. B 15 (1977) 4789.

[22] P. Hohenberg, W. Kohn, Inhomogenous electron gas, Phys. Rev. 136 (1964) B864–B871.

[23] W. Kohn, L.J. Sham, Self-consistent equations including exchange and correlation effects, Phys. Rev. 140 (1965) A1133–A1138.

[24] G. Kresse, J. Furthmüller, Efficiency of ab-initio total energy calculations for metals and semiconductors using a plane-wave basis set, Comput. Mater. Sci. 6 (1996) 15–49.

[25] P. Blaha, K. Schwarz, G. Madsen, D. Kvasnicka, J. Luitz, WIEN2k, an Augmented Plane Wave + Local Orbitals Program for Calculating Crystal Properties, Karlheinz Schwarz, Technische Universtiät Wien, Vienna, Austria, 2001.

[26] X. Gonze, J.-M. Beuken, R. Caracas, F. Detraux, M. Fuchs, G.-M. Rignanese, L. Sindic, M. Verstraete, G. Zerah, F. Jollet, M. Torrent, A. Roy, M. Mikami, Ph Ghosez, J.-Y. Raty, D.C. Allan, First-principles computation of material properties: the ABINIT software project, Comput. Mater. Sci. 25 (2002) 478–491.

[27] P. Giannozzi, S. Baroni, N. Bonini, M. Calandra, R. Car, C. Cavazzoni, D. Ceresoli, G.L. Chiarotti, M. Cococcioni, I. Dabo, A. Dal Corso, S. de Gironcoli, S. Fabris, G. Fratesi, R. Gebauer, U. Gerstmann, C. Gougoussis, A. Kokalj, M. Lazzeri, L. Martin-Samos, N. Marzari, F. Mauri, R. Mazzarello, S. Paolini, A. Pasquarello, L. Paulatto, C. Sbraccia, S. Scandolo, G. Sclauzero, A.P. Seitsonen, A. Smogunov, P. Umari, Re M. Wentzcovitch, QUANTUM ESPRESSO: a modular and open-source software project for quantum simulations of materials, J. Phys. Condens. Matter 21 (2009) 395502–395521.

[28] A. Debernardi, S. Baroni, E. Molinari, Anharmonic phonon lifetimes in semiconductors from density-functional perturbation theory, Phys. Rev. Lett. 75 (1995) 1819–1823.

[29] A. Debernardi, Phonon linewidths in III-V semiconductors from density-functional perturbation theory, Phys. Rev. B 57 (1998) 12847–12858.

[30] A. Debernardi, C. Ulrich, M. Cardona, K. Syassen, Pressure dependence of Raman linewidth in semiconductors, Phys. Status Solidi (b) 223 (2001) 213–224.

[31] G. Deinzer, D. Strauch, Raman tensor calculated from the 2n+1 theorem in density-functional theory, Phys. Rev. B 66 (2002) 100301–100303.

[32] G. Deinzer, G. Birner, D. Strauch, Ab initio calculation of the linewidth of various phonon modes in germanium and silicon, Phys. Rev. B 67 (2003) 144304–144309.

[33] G. Deinzer, M. Schmitt, A.P. Mayer, D. Strauch, Intrinsic lifetimes and anharmonic frequency shifts of long-wavelength optical phonons in polar crystals, Phys. Rev. B 69 (2004) 014304–014310.

[34] N. Bonini, M. Lazzeri, N. Marzari, F. Mauri, Phonon anharmonicities in graphite and graphene, Phys. Rev. Lett. 99 (2007) 176802–176805.

[35] A.J. Giles, S. Dai, I. Vurgaftman, T. Hoffman, S. Liu, L. Lindsay, C.T. Ellis, N. Assefa, I. Chatzakis, T.L. Reinecke, J.G. Tischler, M.M. Fogler, J.H. Edgar, D.N. Basov, J.D. Caldwell, Ultralow-loss polaritons in isotopically pure boron nitride, Nat. Mater. 17 (2018) 134–140.

[36] Q. Zheng, S. Li, C. Li, Y. Lv, X. Liu, P.Y. Huang, D.A. Broido, B. Lv, D.G. Cahill, High thermal conductivity in isotopically enriched cubic boron phosphide, Adv. Funct. Mater. (2018) 1–9, 1805116.

[37] W. Li, N. Mingo, Lattice dynamics and thermal conductivity of skutterdites $CoSb_3$ and $IrSb_3$ from first principles: why $IrSb_3$ is a better thermal conductor than $CoSb_3$, Phys. Rev. B 90 (2014) 094302.

[38] W. Li, J. Carrete, N.A. Katcho, N. Mingo, ShengBTE: a solver of the Boltzmann transport equation for phonons, Comput. Phys. Commun. 185 (2014) 1747–1758.

[39] T. Tadano, Y. Gohda, S. Tsuneyuki, Anharmonic force constants extracted from first-principles molecular dynamics: applications to heat transfer simulations, J. Phys. Condens. Matter 26 (2014) 225402–225413.

[40] A. Togo, L. Chaput, I. Tanaka, Distributions of phonon lifetimes in Brillouin zones, Phys. Rev. B 91 (2015) 094306–094336.

[41] A. Chernatynskiy, S.R. Phillpot, Phonon transport simulator (PhonTS), Comput. Phys. Commun. 192 (2015) 196–203.

[42] X. Tang, J. Dong, Lattice thermal conductivity of MgO at conditions of Earth's interior, PNAS 107 (2010) 4539–4543.

[43] J. Shiomi, K. Esfarjani, G. Chen, Thermal conductivity of half-Heusler compounds from first-principles calculations, Phys. Rev. B 84 (2011) 104302.

[44] G. Leibfried, W. Ludwig, Theory of anharmonic effects in crystals, Solid State Phys. 12 (1961) 275.

[45] L. Lindsay, D.A. Broido, T.L. Reinecke, Ab initio thermal transport in compound semiconductors, Phys. Rev. B 87 (2013) 165201.

[46] S. Lee, K. Esfarjani, T. Luo, J. Zhou, Z. Tian, G. Chen, Resonant bonding leads to low lattice thermal conductivity, Nat. Commun. 5 (2014) 3525.

[47] S. Lee, K. Esfarjani, J. Mendoza, M.S. Dresselhaus, G. Chen, Lattice thermal conductivity of Bi, Sb, and Bi-Sb alloys from first principles, Phys. Rev. B 89 (2014) 085206.

[48] G. Qin, M. Hu, Accelerating evaluation of converged lattice thermal conductivity, npj Comp. Mat. 4 (2018) 3.

[49] P. Haas, F. Tran, P. Blaha, Calculation of the lattice constant of solids with semilocal functionals, Phys. Rev. B 79 (2009) 085104.

[50] A. Jain, A.J.H. McGaughey, Effect of exchange-correlation on first-principles-driven lattice thermal conductivity predictions of crystalline silicon, Comput. Mater. Sci. 110 (2015) 115–120.

[51] A. Taheri, C. Da Silva, C.H. Amon, First-principles phonon thermal transport in graphene: effects of exchange-correlation and type of pseudopotential, J. Appl. Phys. 123 (2018) 215105.

[52] A. Chernatynskiy, S.R. Philpot, Thermal conductivity of argon at high pressure from first principles calculations, J. Appl. Phys. 114 (2013) 064902.

[53] L. Lindsay, W. Li, J. Carrete, N. Mingo, D.A. Broido, T.L. Reinecke, Phonon thermal transport in strained and unstrained graphene from first principles, Phys. Rev. B 89 (2014) 155426.

[54] R. Guo, X. Wang, Y. Kuang, B. Huang, First-principles study of anisotropic thermoelectric transport properties of IV-VI semiconductor compounds SnSe and SnS, Phys. Rev. B 92 (2015) 115202.

[55] L. Feng, T. Shiga, J. Shiomi, Phonon transport in perovskite $SrTiO_3$ from first principles, Appl. Phys. Express 8 (2015) 071501.

[56] L. Lindsay, Isotope scattering and phonon thermal conductivity in light atom compounds: LiH and LiF, Phys. Rev. B 94 (2016) 174304.

[57] Y. Wang, Z. Lu, X. Ruan, First principles calculation of lattice thermal conductivity of metals considering phonon-phonon and phonon-electron scattering, J. Appl. Phys. 119 (2016) 225109.

[58] D. Campi, L. Paulatto, G. Fugallo, F. Mauri, M. Bernasconi, First-principles calculation of lattice thermal conductivity in crystalline phase change materials: GeTe, Sb_2Te_3, and $Ge_2Sb_2Te_5$, Phys. Rev. B 95 (2017) 024311.

[59] R. Guo, X. Wang, B. Huang, Thermal conductivity of skutterudite $CoSb_3$ from first principles: substitution and nanoengineering effects, Sci. Rep. 5 (2015) 7806.

[60] A. Chernatynskiy, S.R. Phillpot, Anharmonic properties in Mg_2X (X=C, Si, Ge, Sn, Pb) from first-principles calculations, Phys. Rev. B 92 (2015) 064303.

[61] J. He, M. Amsler, Y. Xia, S.S. Naghavi, V.I. Hegde, S. Hao, S. Goedecker, V. Ozoliņš, C. Wolverton, Ultralow thermal conductivity in full Heusler semiconductors, Phys. Rev. Lett. 117 (2016) 046602.

[62] J. Carrete, W. Li, N. Mingo, S. Wang, S. Curtarolo, Finding unprecedentedly low-thermal-conductivity half-Heusler semiconductors via high-throughput materials modeling, Phys. Rev. X 4 (2014) 011019.

[63] A. Seko, A. Togo, H. Hayashi, K. Tsuda, L. Chaput, I. Tanaka, Prediction of low-thermal-conductivity compounds with first-principles anharmonic lattice-

dynamics calculations and Bayesian optimization, Phys. Rev. Lett. 115 (2015) 205901.
[64] F. Legrain, J. Carrete, A. van Roekeghem, G.K.H. Madsen, N. Mingo, Materials screening for the discovery of new half-heuslers: machine learning versus Ab initio methods, J. Phys. Chem. B 122 (2017) 625–632.
[65] T. Feng, X. Ruan, Quantum mechanical prediction of four-phonon scattering rates and reduced thermal conductivity of solids, Phys. Rev. B 93 (2016) 045202.
[66] J.E. Turney, E.S. Landry, A.J.H. McGaughey, C.H. Amon, Predicting phonon properties and thermal conductivity from anharmonic lattice dynamics calculations and molecular dynamics simulations, Phys. Rev. B 79 (2009) 064301.
[67] L. Lindsay, D.A. Broido, Three-phonon phase space and lattice thermal conductivity in semiconductors, J. Phys. Condens. Matter 20 (2008) 165209.
[68] P. Sapna, T.J. Singh, Role of three-phonon and four-phonon processes in thermal transport of single-walled carbon nanotubes, Mod. Phys. Lett. B 27 (2013) 1350117.
[69] S.-Y. Yue, X. Zhang, G. Qin, S.R. Phillpot, M. Hu, Metric for strong intrinsic fourth-order phonon anharmonicity, Phys. Rev. B 95 (2017) 195203.
[70] T. Feng, L. Lindsay, X. Ruan, Four-phonon scattering significantly reduces intrinsic thermal conductivity in solids, Phys. Rev. B 96 (2017) 161201.
[71] J.S. Kang, M. Li, H. Wu, H. Nguyen, Y. Hu, Experimental observation of high thermal conductivity in boron arsenide, Science 361 (2018) 575.
[72] S. Li, Q. Zheng, Y. Lv, X. Liu, X. Wang, P.Y. Huang, D.G. Cahill, B. Lv, High thermal conductivity in cubic boron arsenide crystals, Science 361 (2018) 579.
[73] F. Tian, B. Song, X. Chen, N.K. Ravichandran, Y. Lv, K. Chen, S. Sullivan, J. Kim, Y. Zhou, T.-H. Liu, M. Goni, Z. Ding, J. Sun, G.A.U.U. Gamage, H. Sun, H. Ziyaee, S. Huyan, L. Deng, J. Zhou, A.J. Schmidt, S. Chen, C.-W. Chu, P.Y. Huang, D. Broido, L. Shi, G. Chen, Z. Ren, Unusual high thermal conductivity in boron arsenide bulk crystals, Science 361 (2018) 582.
[74] L. Lindsay, D.A. Broido, T.L. Reinecke, First-principles determination of ultrahigh thermal conductivity of boron arsenide: a competitor for diamond? Phys. Rev. Lett. 111 (2013) 025901.
[75] T. Feng, X. Ruan, Four-phonon scattering reduces intrinsic thermal conductivity of graphene and the contributions from flexural phonons, Phys. Rev. B 97 (2018) 045202.
[76] N.K. Ravichandran, D. Broido, Unified first-principles theory of thermal properties of insulators, Phys. Rev. B 98 (2018) 085205.
[77] Y. Xia, Revisiting lattice thermal transport in PbTe: the crucial role of quartic anharmonicity, Appl. Phys. Lett. 113 (2018) 073901.
[78] F. Giustino, M.L. Cohen, S.G. Louie, Electron-phonon interaction using Wannier functions, Phys. Rev. B 76 (2007) 165108.
[79] J. Noffsinger, F. Giustino, B.D. Malone, C.-H. Park, S.G. Louie, M.L. Cohen, EPW: a program for calculating the electron–phonon coupling using maximally localized Wannier functions, Comput. Phys. Commun. 181 (2010) 2140–2148.
[80] S. Poncé, E.R. Margine, C. Verdi, F. Giustino, EPW: electron–phonon coupling, transport and superconducting properties using maximally localized Wannier functions, Comput. Phys. Commun. 209 (2016) 116–133.
[81] J. Zhou, B. Liao, G. Chen, First-principles calculations of thermal, electrical, and thermoelectric transport properties of semiconductors, Semicond. Sci. Technol. 31 (2016) 043001.
[82] T.-H. Liu, J. Zhou, B. Liao, D.J. Singh, G. Chen, First-principles mode-by-mode analysis for electron-phonon scattering channels and mean free path spectra in GaAs, Phys. Rev. B 95 (2017) 075206.
[83] B. Liao, B. Qiu, J. Zhou, S. Huberman, K. Esfarjani, G. Chen, Significant reduction of lattice thermal conductivity by the electron-phonon interaction in silicon with high carrier concentrations: a first-principles study, Phys. Rev. Lett. 114 (2015) 115901.
[84] A. Jain, A.J.H. McGaughey, Thermal transport by phonons and electrons in aluminum, silver, and gold from first principles, Phys. Rev. B 93 (2016) 081206.
[85] C. Li, N.K. Ravichandran, L. Lindsay, D. Broido, Fermi surface nesting and phonon frequency gap drive anomalous thermal transport, Phys. Rev. Lett. 121 (2018) 175901.
[86] A. Togo, I. Tanaka, First principles phonon calculations in materials science, Scripta Mater. 108 (2015) 1–5.
[87] J.M. Skelton, S.C. Parker, A. Togo, I. Tananka, A. Walsh, Thermal physics of the lead chalcogenides PbS, PbSe, and PbTe from first principles, Phys. Rev. B 89 (2014) 205203.
[88] O. Hellman, I.A. Abrikosov, S.I. Simak, Lattice dynamics of anharmonic solids from first principles, Phys. Rev. B 84 (2011) 180301–180304.
[89] O. Hellman, I.A. Abrikosov, Temperature-dependent effective third-order interatomic force constants from first principles, Phys. Rev. B 88 (2013) 144301–144306.
[90] F. Zhou, W. Nielson, Y. Xia, V. Ozoliņš, Lattice anharmonicity and thermal conductivity from compressive sensing of first-principles calculations, Phys. Rev. Lett. 113 (2014) 185501.
[91] N.R. Werthamer, Self-consistent phonon formulation of anharmonic lattice dynamics, Phys. Rev. B 1 (1970) 572.
[92] T. Tadano, S. Tsuneyuki, Self-consistent phonon calculations of lattice dynamical properties in cubic $SrTiO_3$ with first-principles anharmonic force constants, Phys. Rev. B 92 (2015) 054301.
[93] C.W. Li, O. Hellman, J. Ma, A.F. May, H.B. Cao, X. Chen, A.D. Christianson, G. Ehlers, D.J. Singh, B.C. Sales, O. Delaire, Phonon self-energy and origin of anomalous neutron scattering spectra in SnTe and PbTe thermoelectrics, Phys. Rev. Lett. 112 (2014) 175501.
[94] A.H. Romero, E.K.U. Gross, M.J. Verstraete, O. Hellman, Thermal conductivity in PbTe from first principles, Phys. Rev. B 91 (2015) 214310.
[95] A.L. Miranda, B. Xu, O. Hellman, A.H. Romero, M.J. Verstraete, Ab initio calculation of the thermal conductivity of indium antimonide, Semicond. Sci. Technol. 29 (2014) 124002.
[96] O. Hellman, D.A. Broido, Phonon thermal transport in Bi_2Te_3 from first principles, Phys. Rev. B 90 (2014) 134309.
[97] A. van Roekeghem, J. Carrete, N. Mingo, Anomalous thermal conductivity and suppression of negative thermal expansion in ScF_3, Phys. Rev. B 94 (2016) 020303.
[98] D.A. Broido, L. Lindsay, A. Ward, Thermal conductivity of diamond under extreme pressure: a first-principles study, Phys. Rev. B 86 (2012) 115203.
[99] S. Mukhopadhyay, D.A. Stewart, Polar effects on the thermal conductivity of cubic boron nitride under pressure, Phys. Rev. Lett. 113 (2014) 025901.
[100] L. Lindsay, D.A. Broido, J. Carrete, N. Mingo, T.L. Reinecke, Anomalous pressure dependence of thermal conductivities of large mass ratio compounds, Phys. Rev. B 91 (2015) 121202.
[101] T. Ouyang, M. Hu, Competing mechanism driving diverse pressure dependence of thermal conductivity of XTe (X=Hg, Cd, and Zn), Phys. Rev. B 92 (2015) 235204.
[102] S. Mukhopadhyay, D. Bansal, O. Delaire, D. Perrodin, E. Bourret-Courchesne, D.J. Singh, L. Lindsay, The curious case of cuprous chloride: giant thermal resistance and anharmonic quasiparticle spectra driven by dispersion nesting, Phys. Rev. B 96 (2017) 100301.
[103] Y. Kuang, L. Lindsay, S. Shi, X. Wang, B. Huang, Thermal conductivity of graphene mediated by strain and size, Int. J. Heat Mass Tran. 101 (2016) 772–778.
[104] H. Xie, Large tunability of lattice thermal conductivity of monolayer silicene via mechanical strain, Phys. Rev. B 93 (2016) 075404.
[105] Y. Kuang, L. Lindsay, B. Huang, Unusual enhancement in intrinsic thermal conductivity of multilayer graphene by tensile strains, Nano Lett. 15 (2015) 6121–6127.
[106] L. Zhu, T. Zhang, Z. Sun, J. Li, G. Chen, S.A. Yang, Thermal conductivity of biaxial-strained MoS_2: sensitive strain dependence and size-dependent reduction rate, Nanotechnology 26 (2015) 465707.
[107] G.A. Slack, Nonmetallic crystals with high thermal conductivity, J. Phys. Chem. Solid. 34 (1973) 321.
[108] D.T. Morelli, G.A. Slack, in: S. Shinde, J. Goela (Eds.), High Thermal Conductivity Materials, Springer, New York, 2005, p. 37.
[109] L. Lindsay, D.A. Broido, T.L. Reinecke, Thermal conductivity and large isotope effect in GaN from first principles, Phys. Rev. Lett. 109 (2012) 095901.
[110] A. Jain, A.J.H. McGaughey, Thermal conductivity of compound semiconductors: interplay of mass density and acoustic-optical phonon frequency gap, J. Appl. Phys. 116 (2014) 073503.
[111] D.A. Broido, L. Lindsay, T.L. Reinecke, Ab initio study of the unusual thermal transport properties of boron arsenide and related materials, Phys. Rev. B 88 (2013) 214303.
[112] S. Mukhopadhyay, L. Lindsay, D.S. Parker, Optic phonon bandwidth and lattice thermal conductivity: the case of Li_2X (X=O, S, Se, Te), Phys. Rev. B 93 (2016) 224301.
[113] J. Garg, T. Luo, G. Chen, Spectral concentration of thermal conductivity in GaN – a first-principles study, Appl. Phys. Lett. 112 (2018) 252101.
[114] A. Katre, J. Carrete, T. Wang, G.K.H. Madsen, N. Mingo, Phonon transport unveils the prevalent point defects in GaN, Phys. Rev. Mat. 2 (2018) 50602.
[115] X. Wu, J. Lee, V. Varshney, J.L. Wohlwend, A.K. Roy, T. Luo, Thermal conductivity of wurtzite zinc-oxide from first-principles lattice dynamics – a comparative study with gallium nitride, Sci. Rep. 6 (2016) 22504.
[116] A. Katre, J. Carette, B. Dongre, G.K.H. Madsen, N. Mingo, Exceptionally strong phonon scattering by B substitution in cubic SiC, Phys. Rev. Lett. 119 (2017) 075902.
[117] N.H. Protik, A. Katre, L. Lindsay, J. Carrete, N. Mingo, D. Broido, Phonon thermal transport in 2H, 4H and 6H silicon carbide from first principles, Mat. Today Phys. 1 (2017) 31–38.
[118] P. Chakraborty, G. Xiong, L. Cao, Y. Wang, Lattice thermal transport in superhard hexagonal diamond and wurtzite boron nitride: a comparative study with cubic diamond and cubic boron nitride, Carbon 139 (2018) 85–93.
[119] R.G. Greene, H. Luo, A.L. Ruoff, S.S. Trail, F.I. DiSalvo, Phys. Rev. Lett. 73 (1994) 2476.
[120] V.G. Hadjiev, M.N. Iliev, B. Lv, Z.F. Ren, C.W. Chu, Anomalous vibrational properties of cubic boron arsenide, Phys. Rev. B 89 (2014) 024308.
[121] H. Ma, C. Li, S. Tang, J. Yan, A. Alatas, L. Lindsay, B.C. Sales, Z. Tian, Boron arsenide phonon dispersion from inelastic x-ray scattering: potential for ultrahigh thermal conductivity, Phys. Rev. B 94 (2016) 220303.
[122] B. Lv, Y. Lan, X. Wang, Q. Zhang, Y. Hu, A.J. Jacobson, D. Broido, G. Chen, Z. Ren, C.-W. Chu, Experimental study of the proposed super-thermal conductor: BAs, Appl. Phys. Lett. 106 (2015) 074105.
[123] J. Kim, D.A. Evans, D.P. Sellan, O.M. Williams, E. Ou, A.H. Cowley, L. Shi, Thermal and thermoelectric transport measurements of an individual boron arsenide microstructure, Appl. Phys. Lett. 108 (2016) 201905.

[124] F. Tian, B. Song, B. Lv, J. Sun, S. Huyan, Q. Wu, J. Mao, Y. Ni, Z. Ding, S. Huberman, T.-H. Liu, G. Chen, S. Chen, C.-W. Chu, Z. Ren, Seeded growth of boron arsenide single crystals with high thermal conductivity, Appl. Phys. Lett. 112 (2018) 031903.

[125] N.H. Protik, J. Carrete, N.A. Katcho, N. Mingo, D. Broido, Ab initio study of the effect of vacancies on the thermal conductivity of boron arsenide, Phys. Rev. B 94 (2016) 045207.

[126] Q. Zheng, C.A. Polanco, M.-H. Du, L.R. Lindsay, M. Chi, J. Yan, B.C. Sales, Antisite pairs suppress the thermal conductivity of BAs, Phys. Rev. Lett. 121 (2018) 105901.

[127] J. Garg, N. Bonini, B. Kozinsky, N. Marzari, Role of disorder and anharmonicity in the thermal conductivity of silicon-germanium alloys: a first-principles study, Phys. Rev. Lett. 106 (2011) 045901.

[128] Z. Tian, K. Esfarjani, G. Chen, Enhancing phonon transmission across a Si/Ge interface by atomic roughness: first-principles study with the Green's function method, Phys. Rev. B 86 (2012) 235304.

[129] Z. Tian, K. Esfarjani, G. Chen, Green's function studies of phonon transport across Si/Ge superlattices, Phys. Rev. B 89 (2014) 235307.

[130] O. Delaire, J. Ma, K. Marty, A.F. May, M.A. McGuire, M.-H. Du, D.J. Singh, A. Podlesnyak, G. Ehlers, M.D. Lumsden, B.C. Sales, Giant anharmonic phonon scattering in PbTe, Nat. Mater. 10 (2011) 614–619.

[131] Y. Zhang, X. Ke, P.R.C. Kent, J. Yang, C. Chen, Anomalous lattice dynamics near the ferroelectric instability in PbTe, Phys. Rev. Lett. 107 (2011) 175503.

[132] Z. Tian, M. Li, Z. Ren, H. Ma, A. Alatas, S.D. Wilson, J. Li, Inelastic x-ray scattering measurements of phonon dispersion and lifetimes in $PbTe_{1-x}Se_x$ alloys, J. Phys. Condens. Matter 27 (2015) 375403.

[133] N. Shulumba, O. Hellman, A.J. Minnich, Intrinsic localized mode and low thermal conductivity of PbSe, Phys. Rev. B 95 (2016) 014302.

[134] Y. Xie, Y. Zhou, X.-G. Gong, The intrinsic low lattice thermal conductivity in the rock salt SnSe, Comput. Mater. Sci. 148 (2018) 54–59.

[135] W. Li, N. Mingo, Thermal conductivity of fully filled skutterudites: role of the filler, Phys. Rev. B 89 (2014) 184304.

[136] W. Li, N. Mingo, Ultralow lattice thermal conductivity of the fully filled skutterudite $YbFe_4Sb_{12}$ due to the flat avoided-crossing filler modes, Phys. Rev. B 91 (2015) 144304.

[137] T. Tadano, Y. Gohda, S. Tsuneyuki, Impact of rattlers on thermal conductivity of a thermoelectric clathrate: a first principles study, Phys. Rev. Lett. 114 (2015) 095501.

[138] H. Euchner, S. Paihès, V.M. Giordano, M. de Boissieu, Understanding lattice thermal conductivity in thermoelectric clathrates: a density functional theory study on binary Si-based type-I clathrates, Phys. Rev. B 97 (2018) 014304.

[139] C. Chen, Z. Zhang, J. Chen, Revisit to the impacts of rattlers on thermal conductivity of clathrates, Front. Energy Res. 6 (2018) 34.

[140] S. Kerdsongpanya, O. Hellman, B. Sun, Y.K. Koh, J. Lu, N.V. Nong, S.I. Simak, B. Alling, P. Eklund, Phonon thermal conductivity of scandium nitride for thermoelectrics from first-principles calculations and thin-film growth, Phys. Rev. B 96 (2017) 195417.

[141] J.O. Morales-Ferreiro, D.E. Diaz-Droguett, D. Celentano, T. Luo, First-principles calculations of thermoelectric properties of IV-VI chalcogenides 2D materials, Front. Mech. Eng. 3 (2017) 15.

[142] Y. Zhang, J. Dong, P.R.C. Kent, J. Yang, C. Chen, Intrinsic low thermal conductivity in weakly ionic rocksalt structures, Phys. Rev. B 92 (2015) 020301.

[143] T. Ouyang, M. Hu, First-principles study on lattice thermal conductivity of thermoelectrics HgTe in different phases, J. Appl. Phys. 117 (2015) 245101.

[144] Y.-Y. Qi, T. Zhang, Y. Cheng, X.-R. Chen, D.-Q. Wei, L.-C. Cai, Lattice dynamics and thermal conductivity of calcium fluoride via first-principles investigation, J. Appl. Phys. 119 (2016) 095103.

[145] S. Yabuuchi, Y. Kurosaki, A. Nishide, N. Fukatani, J. Hayakawa, First-principles study on thermoelectric transport properties of Ca_3Si_4, Phys. Rev. Mat. 1 (2017) 045405.

[146] G. Ding, J. Carrete, W. Li, G.Y. Gao, K. Yao, Ultralow lattice thermal conductivity in topological insulator $TlBiSe_2$, Appl. Phys. Lett. 108 (2016) 233902.

[147] Y. Fu, X. He, L. Zhang, D.J. Singh, Collective-Goldstone-mode-induced ultralow lattice thermal conductivity in Sn-filled skutterudite $SnFe_4Sb_{12}$, Phys. Rev. B 97 (2018) 024301.

[148] W. Li, J. Carrete, G.K.H. Madsen, N. Mingo, Influence of the optical-acoustic phonon hybridization on phonon scattering and thermal conductivity, Phys. Rev. B 93 (2016) 205203.

[149] Y. Fu, D.J. Singh, W. Li, L. Zhang, Intrinsic ultralow lattice thermal conductivity of the unfilled skutterudite $FeSb_3$, Phys. Rev. B 94 (2016) 075122.

[150] H.S. Ji, A. Togo, M. Kaviany, I. Tanaka, J.H. Shim, Low phonon conductivity of layered BiCuOS, BiCuOSe, and BiCuOTe from first principles, Phys. Rev. B 94 (2016) 115203.

[151] T. Pandey, A.K. Singh, High thermopower and ultralow thermal conductivity in Cd-based Zintl phase compounds, Phys. Chem. Chem. Phys. 17 (2015) 16917.

[152] Y. Fu, D.J. Singh, Thermal conductivity of perovskite $KTaO_3$ and $PbTiO_3$ from first principles, Phys. Rev. Mat. 2 (2018) 094408.

[153] M.D. Santia, N. Tandon, J.D. Albrecht, Lattice thermal conductivity in β-Ga_2O_3 from first principles, Appl. Phys. Lett. 107 (2015) 041907.

[154] S. Mukhopadhyay, L. Lindsay, D.J. Singh, Optic phonons and anisotropic thermal conductivity in hexagonal $Ge_2Sb_2Te_5$, Sci. Rep. 6 (2016) 37076.

[155] L. Lindsay, Y. Kuang, Effects of functional group mass variance on vibrational properties and thermal transport in graphene, Phys. Rev. B 95 (2017) 121404.

[156] J.H. Seol, I. Jo, A.L. Moore, L. Lindsay, Z.H. Aitken, M.T. Pettes, X. Li, Z. Yao, R. Huang, D. Broido, N. Mingo, R.S. Ruoff, L. Shi, Two-dimensional phonon transport in supported graphene, Science 328 (2010) 213–216.

[157] L. Lindsay, D.A. Broido, N. Mingo, Flexural phonons and thermal transport in graphene, Phys. Rev. B 82 (2010) 115427.

[158] A.A. Balandin, S. Ghosh, W. Bao, I. Calizo, D. Teweldebrhan, F. Miao, C.N. Lau, Superior thermal conductivity of single-layer graphene, Nano Lett. 8 (2008) 902.

[159] W. Cai, A.L. Moore, Y. Zhu, X. Li, S. Chen, L. Shi, R.S. Ruoff, Thermal transport in suspended and supported monolayer graphene grown by chemical vapor deposition, Nano Lett. 10 (2010) 1645.

[160] J.-U. Lee, D. Yoon, H. Kim, S.W. Lee, H. Cheong, Thermal conductivity of suspended pristine graphene measured by Raman spectroscopy, Phys. Rev. B 83 (2011) 081419.

[161] S. Chen, Q. Wu, C. Mishra, J. Kang, H. Zhang, K. Cho, W. Cai, A.A. Balandin, R.S. Ruoff, Thermal conductivity of isotopically modified graphene, Nat. Mater. 11 (2012) 203.

[162] S. Lee, D.A. Broido, K. Esfarjani, G. Chen, Hydrodynamic phonon transport in suspended graphene, Nat. Commun. 6 (2015) 6290–6299.

[163] A. Cepellotti, G. Fugallo, L. Paulatto, M. Lazzeri, F. Mauri, N. Marzari, Phonon hydrodynamics in two-dimensional materials, Nat. Commun. 6 (2015) 6400–6406.

[164] N. Bonini, J. Garg, N. Marzari, Acoustic phonon lifetimes and thermal transport in free-standing and strained graphene, Nano Lett. 12 (2012) 2673–2678.

[165] X. Wu, V. Varshney, J. Lee, Y. Pang, A.K. Roy, T. Luo, How to characterize thermal transport capability of 2D materials fairly? – sheet thermal conductance and the choice of thickness, Chem. Phys. Lett. 669 (2017) 233.

[166] X. Xu, L.F.C. Pereira, Y. Wang, J. Wu, K. Zhang, X. Zhao, S. Bae, C.T. Bui, R. Xie, J.T.L. Thong, B.H. Hong, K.P. Loh, D. Donadio, B. Li, B. Özyilmaz, Length-dependent thermal conductivity in suspended single-layer graphene, Nat. Commun. 5 (2014) 3689.

[167] L. Zhu, G. Zhang, B. Li, Coexistence of size-dependent and size-independent thermal conductivities in phosphorene, Phys. Rev. B 90 (2014) 214302.

[168] W. Li, J. Carrete, N. Mingo, Thermal conductivity and phonon linewidths of monolayer MoS_2 from first principles, Appl. Phys. Lett. 103 (2013) 253103.

[169] A.N. Gandi, U. Schwingenshclögl, Thermal conductivity of bulk and monolayer MoS_2, Europhys. Lett. 113 (2016) 36002.

[170] W.-X. Zhou, K.-Q. Chen, First-principles determination of ultralow thermal conductivity of monolayer WSe_2, Sci. Rep. 5 (2015) 15070.

[171] J. Ma, Y. Chen, Z. Han, W. Li, Strong anisotropic thermal conductivity of monolayer WTe_2, 2D Mater. 3 (2016) 045010.

[172] A. Jain, A.J. McGaughey, Strongly anisotropic in-plane thermal transport in single-layer black phosphorene, Sci. Rep. 5 (2015) 8501.

[173] G. Qin, Anisotropic intrinsic lattice thermal conductivity of phosphorene from first principles, Phys. Chem. Chem. Phys. 17 (2015) 4854.

[174] X. Gu, R. Yang, First-principles prediction of phononic thermal conductivity of silicene: a comparison with graphene, J. Appl. Phys. 117 (2015) 025102.

[175] S.S. Naghavi, J. He, Y. Xia, C. Wolverton, Pd_2Se_3 monolayer: a promising two-dimensional thermoelectric material with ultralow lattice thermal conductivity and high power factor, Chem. Mater. 30 (2018) 5639–5647.

[176] A.S. Nissimagoudar, J. Ma, Y. Chen, W. Li, Thermal transport in monolayer InSe, J. Phys. Condens. Matter 29 (2017) 335702.

[177] T. Pandey, D.S. Parker, L. Lindsay, Ab initio phonon thermal transport in monolayer InSe, GaSe, GaS, and alloys, Nanotechnology 28 (2017) 455706.

[178] A.N. Gandi, H.N. Alshareef, U. Schwingenschlögl, Thermoelectric performance of the MXenes M_2Co_2 (M=Ti,Zr,or Hf), Chem. Mater. 28 (2016) 1647.

[179] A.N. Gandi, H.N. Alshareef, U. Schwingenschlögl, Thermal response in van der Waals heterostructures, J. Phys. Condens. Matter 29 (2017) 035504.

[180] J. Carrete, W. Li, L. Lindsay, D.A. Broido, L.J. Gallego, N. Mingo, Physically founded phonon dispersions of few-layer materials and the case of borophene, Math. Res. Lett. 4 (2016) 204–211.

[181] H. Xiao, W. Cao, T. Ouyang, S. Guo, C. He, J. Zhong, Lattice thermal conductivity of borophene from first principle calculation, Sci. Rep. 7 (2017) 45986.

[182] G. Liu, H. Wang, Y. Gao, J. Zhou, H. Wang, Anisotropic intrinsic lattice thermal conductivity of borophane from first-principles calculations, Phys. Chem. Chem. Phys. 19 (2017) 2843–2849.

[183] S.-Y. Yue, T. Ouyang, M. Hu, Diameter dependence of lattice thermal conductivity of single-walled carbon nanotubes: study from ab initio, Sci. Rep. 5 (2015) 15440.

[184] X. Wang, M. Kaviany, B. Huang, Phonon coupling and transport in individual polyethylene chains: a comparison study with the bulk crystal, Nanoscale 9 (2017) 18022.

[185] Q. Zhang, C. Liu, X. Liu, J. Liu, Z. Cui, Y. Zhang, L. Yang, Y. Zhao, T.T. Xu, Y. Chen, J. Wei, Z. Mao, D. Li, Thermal transport in quasi-1D van der Waals crystal $Ta_2Pd_3Se_8$ nanowires: size and length dependence, ACS Nano 12 (2018) 2634.

[186] T. Pandey, C.A. Polanco, V.R. Cooper, D.S. Parker, L. Lindsay, Symmetry-driven phonon chirality and transport in 1D and bulk Ba_3N-derived materials, Phys. Rev. B 98 (2018) 241405.

[187] L. Lindsay, D.A. Broido, N. Mingo, Lattice thermal conductivity of single-walled carbon nanotubes: beyond the relaxation time approximation and phonon-phonon scattering selection rules, Phys. Rev. B 80 (2009) 125407.
[188] M. Maldovan, Phonon wave interference and thermal bandgap materials, Nat. Mater. 14 (2015) 667.
[189] J. Garg, N. Bonini, N. Marzari, High thermal conductivity in short-period superlattices, Nano Lett. 11 (2011) 5135.
[190] J. Garg, G. Chen, Minimum thermal conductivity in superlattices: a first-principles formalism, Phys. Rev. B 87 (2013) 140302.
[191] P. Chen, N.A. Katcho, J.P. Feser, W. Li, M. Glaser, O.G. Schmidt, D.G. Cahill, N. Mingo, A. Rastelli, Role of surface-segregation-driven intermixing on the thermal transport through planar Si/Ge superlattices, Phys. Rev. Lett. 111 (2013) 115901.
[192] L. Thumfart, J. Carrete, B. Vermeersch, N. Ye, T. Truglas, J. Feser, H. Groiss, N. Mingo, A. Rastelli, Thermal transport through Ge-rich Ge/Si superlattices grown on Ge(001), J. Phys. D Appl. Phys. 51 (2018) 014001.
[193] M.N. Luckyanova, J. Garg, K. Esfarjani, A. Jandl, M.T. Bulsara, A.J. Schmidt, A.J. Minnich, S. Chen, M.S. Dresselhaus, Z. Ren, E.A. Fitzgerald, G. Chen, Coherent phonon heat conduction in superlattices, Science 338 (2012) 936.
[194] M.N. Luckyanova, J.A. Johnson, A.A. Maznev, J. Garg, A. Jandl, M.T. Bulsara, E.A. Fitzgerald, K.A. Nelson, G. Chen, Anisotropy of the thermal conductivity in GaAs/AlAs superlattices, Nano Lett. 13 (2013) 3973–3977.
[195] J. Carrete, B. Vermeersch, L. Thumfart, R.R. Kakodkar, G. Trevisi, P. Frigeri, L. Seravalli, J.P. Feser, A. Rastelli, N. Mingo, Predictive design and experimental realization of InAs/GaAs superlattices with tailored thermal conductivity, J. Phys. Chem. C 122 (2018) 4054–4062.
[196] A. Jain, Y.-J. Yu, A.J.H. McGaughey, Phonon transport in periodic silicon nanoporous films with feature sizes greater than 100 nm, Phys. Rev. B 87 (2013) 195301.
[197] G. Romano, K. Esfarjani, D.A. Strubbe, D. Broido, A.M. Kolpak, Temperature-dependent thermal conductivity in silicon nanostructured materials studied by the Boltzmann transport equation, Phys. Rev. B 93 (2016) 035408.
[198] Y. Hu, L. Zeng, A.J. Minnich, M.S. Dresselhaus, G. Chen, Spectral mapping of thermal conductivity through nanoscale ballistic transport, Nat. Nanotechnol. 10 (2015) 701–706.
[199] W. Li, N. Mingo, L. Lindsay, D.A. Broido, D.A. Stewart, N.A. Katcho, Thermal conductivity of diamond nanowires from first principles, Phys. Rev. B 85 (2012) 195436.
[200] S.-I. Tamura, Isotope scattering of large-wave-vector phonons in GaAs and InSb: deformation-dipole and overlap-shell models, Phys. Rev. B 30 (1984) 849.
[201] L. Lindsay, D.A. Broido, T.L. Reinecke, Phonon-isotope scattering and thermal conductivity in materials with a large isotope effect: a first-principles study, Phys. Rev. B 88 (2013) 144306.
[202] T.R. Anthony, W.F. Banholzer, J.F. Fleischer, L. Wei, P.K. Kuo, R.L. Thomas, R.W. Pryor, Thermal diffusivity of isotopically enriched ^{12}C diamond, Phys. Rev. B (1990) 1104.
[203] N.A. Katcho, J. Carrete, W. Li, N. Mingo, Effect of nitrogen and vacancy defects on the thermal conductivity of diamond: an ab initio Green's function approach, Phys. Rev. B 90 (2014) 094117.
[204] C.A. Polanco, L. Lindsay, Ab initio phonon point defect scattering and thermal transport in graphene, Phys. Rev. B 97 (2018) 014303.
[205] C.A. Polanco, L. Lindsay, Thermal conductivity of InN with point defects from first principles, Phys. Rev. B 98 (2018) 014306.
[206] N. Mingo, K. Esfarjani, D.A. Broido, D.A. Stewart, Cluster scattering effects on phonon conduction in graphene, Phys. Rev. B 81 (2010) 045408.
[207] R. Stern, T. Wang, J. Carrete, N. Mingo, G.K.H. Madsen, Influence of point defects on the thermal conductivity in FeSi, Phys. Rev. B 97 (2018) 195201.
[208] T. Wang, J. Carrete, A. van Roekeghem, N. Mingo, G.K.H. Madsen, Ab initio phonon scattering by dislocations, Phys. Rev. B 95 (2017) 245304.
[209] J. Zhang, C.A. Polanco, A.W. Ghosh, Optimizing the interfacial thermal conductance at gold-alkane junctions from 'first principles', J. Heat Tran. 140 (2018) 092405.
[210] S. Sadasivam, U.V. Waghmare, T.S. Fisher, Electron-phonon coupling and thermal conductance at a metal-semiconductor interface: first-principles analysis, J. Appl. Phys. 117 (2015) 134502.
[211] S. Sadasivam, N. Ye, J.P. Feser, J. Charles, K. Miao, T. Kubis, T.S. Fisher, Thermal transport across metal silicide-silicon interfaces: first-principles calculations and Green's function transport simulations, Phys. Rev. B 95 (2017) 085310.
[212] Y. Xia, J.M. Hodges, M.G. Kanatzidis, M.K.Y. Chan, Lattice thermal transport in group II-alloyed PbTe, Appl. Phys. Lett. 112 (2018) 181906.
[213] L. Lindsay, D.S. Parker, Calculated transport properties of CdO: thermal conductivity and thermoelectric power factor, Phys. Rev. B 92 (2015) 144301.
[214] Z. Zheng, X. Su, R. Deng, C. Stoumpos, H. Xie, W. Liu, Y. Yan, S. Hao, C. Uher, C. Wolverton, M.G. Kanatzidis, X. Tang, Rhobohedral to cubic conversion of GeTe via MnTe alloying leads to ultralow thermal conductivity, electronic band convergence, and high thermoelectric performance, J. Am. Chem. Soc. 140 (2018) 2673–2686.
[215] A. Kundu, N. Mingo, D.A. Broido, D.A. Stewart, Role of light and heavy embedded nanoparticles on the thermal conductivity of SiGe alloys, Phys. Rev. B 84 (2011) 125426.
[216] M. Arrigoni, J. Carrete, N. Mingo, G.K.H. Madsen, First-principles quantitative prediction of the lattice thermal conductivity in random semiconductor alloys: the role of force-constant disorder, Phys. Rev. B 98 (2018) 115205.
[217] Y. Zhao, K.T.E. Chua, C.K. Gan, J. Zhang, B. Peng, Z. Peng, Q. Xiong, Phonons in Bi_2S_3 nanostructures: Raman scattering and first-principles studies, Phys. Rev. B 84 (2011) 205330.
[218] L. Liang, V. Meunier, First-principles Raman spectra of MoS_2, WS_2 and their heterostructures, Nanoscale 6 (2014) 5394–5401.
[219] M.A. Pérez-Osorio, Q. Lin, R.T. Phillips, R.L. Milot, L.M. Herz, M.B. Johnson, F. Giustino, Raman spectrum of the organic-inorganic halide perovskite $CH_3NH_3PbI_3$ from first principles and high-resolution low-temperature Raman measurements, J. Phys. Chem. C 122 (2018) 21703–21717.
[220] S. Mukhopadhyay, D.S. Parker, B.C. Sales, A.A. Puretzky, M.A. McGuire, L. Lindsay, Two-channel model for ultralow thermal conductivity of crystalline Tl_3VSe_4, Science 360 (2018) 1455.
[221] R. Yan, J.R. Simpson, S. Bertolazzi, J. Brivio, M. Watson, X. Wu, A. Kis, T. Luo, A.R.H. Walker, J.G. Xing, Thermal conductivity of monolayer molybdenum disulfide obtained from temperature-dependent Raman spectroscopy, ACS Nano 8 (2014) 986–993.
[222] J.W.L. Pang, W.J.L. Buyers, A. Chernatynskiy, M.D. Lumsden, B.C. Larson, S.R. Phillpot, Phonon lifetime investigation of anharmonicity and thermal conductivity of UO_2 by neutron scattering and theory, Phys. Rev. Lett. 110 (2013) 157401.
[223] J.A. Johnson, A.A. Maznev, M.T. Bulsara, E.A. Fitzgerald, T.C. Harman, S. Calawa, C.J. Vineis, G. Turner, K.A. Nelson, Phase-controlled, heterodyne laser-induced transient grating measurements of thermal transport properties in opaque material, J. Appl. Phys. 111 (2012) 023503.
[224] J. Lee, E. Bozorg-Grayeli, S.-B. Kim, M. Asheghi, H.-S.P. Wong, K.E. Goodson, Phonon and electron transport through $Ge_2Sb_2Te_5$ films and interfaces bounded by metals, Appl. Phys. Lett. 102 (2013) 191911.
[225] R. Cheaito, J.T. Gaskins, M.E. Caplan, B.F. Donovan, B.M. Foley, A. Giri, J.C. Duda, C.J. Szwejkowski, C. Constantin, H.J. Brown-Shaklee, J.F. Ihlefeld, P.E. Hopkins, Thermal boundary conductance accumulation and interfacial phonon transmission: measurements and theory, Phys. Rev. B 91 (2015) 035432.
[226] R. Wilson, D. Cahill, Anisotropic failure of Fourier theory in time-domain thermoreflectance experiments, Nat. Commun. 5 (2014) 5075.
[227] J.P. Feser, D.G. Cahill, Probing anisotropic heat transport using time-domain thermoreflectance with offset laser spots, Rev. Sci. Instrum. 83 (2012) 104901.
[228] D. Rodin, S.K. Yee, Simultaneous measurement of in-plane and through-plane thermal conductivity using beam-offset frequency domain thermoreflectance, Rev. Sci. Instrum. 88 (2017) 014902.
[229] P. Jiang, B. Huang, Y.K. Koh, Accurate measurements of cross-plane thermal conductivity of thin films by dual-frequency time-domain thermoreflectance (TDTR), Rev. Sci. Instrum. 87 (2016) 075101.
[230] Z. Wang, J.E. Alaniz, W. Jang, J.E. Garay, C. Dames, Thermal conductivity of nanocrystalline silicon: importance of grain size and frequency-dependent mean free paths, Nano Lett. 11 (2011) 2206–2213.
[231] G. Chen, Nanoscale Energy Transport and Conversion: a Parallel Treatment of Electrons, Molecules, Phonons, and Photons, Oxford University Press, 2005.
[232] A. Majumdar, Microscale heat conduction in dielectric thin films, J. Heat Tran. 115 (1993) 7–16.
[233] J.A. Johnson, A.A. Maznev, J. Cuffe, J.K. Eliason, A.J. Minnich, T. Kehoe, C.M. Sotomayor Torres, G. Chen, K.A. Nelson, Direct measurement of room-temperature nondiffusive thermal transport over micron distances in a silicon membrane, Phys. Rev. Lett. 110 (2013) 025901.
[234] N.K. Ravichandran, H. Zhang, A.J. Minnich, Spectrally resolved specular reactions of thermal phonons from atomically rough surfaces, Phys. Rev. X 8 (2018) 041004.
[235] Y.K. Koh, D.G. Cahill, Frequency dependence of the thermal conductivity of semiconductor alloys, Phys. Rev. B 76 (2007) 075207.
[236] A.J. Minnich, J.A. Johnson, A.J. Schmidt, K. Esfarjani, M.S. Dresselhaus, K.A. Nelson, G. Chen, Thermal conductivity spectroscopy technique to measure phonon mean free paths, Phys. Rev. Lett. 107 (2011) 095901.
[237] T.S. English, L.M. Phinney, P.E. Hopkins, J.R. Serrano, Mean free path effects on the experimentally measured thermal conductivity of single-crystal silicon microbridges, J. Heat Tran. 135 (2013) 091103.
[238] D. Ding, X. Chen, A.J. Minnich, Radial quasiballistic transport in time-domain thermoreflectance studied using Monte Carlo simulations, Appl. Phys. Lett. 104 (2015) 143104.
[239] K. Regner, D. Sellan, Z. Su, C. Amon, A. McGaughey, J. Malen, Broadband phonon mean free path contributions to thermal conductivity measured using frequency-domain thermoreflectance, Nat. Commun. 4 (2013) 1640.
[240] C. Hua, X. Chen, N.K. Ravichandran, A.J. Minnich, Experimental metrology to obtain thermal phonon transmission coefficients at solid interfaces, Phys. Rev. B 95 (2017) 205423.
[241] M. Highland, B.C. Gundrum, Y.K. Koh, R.S. Averback, D.G. Cahill, V.C. Elarde, J.J. Coleman, D.A. Walko, E.C. Landahl, Ballistic-phonon heat conduction at the nanoscale as revealed by time-resolved x-ray diffraction and time-domain thermoreflectance, Phys. Rev. B 76 (2007) 075337.
[242] M.E. Siemens, Q. Li, R. Yang, K.A. Nelson, E.H. Anderson, M.M. Murnane, H.C. Kapteyn, Quasi-ballistic thermal transport from nanoscale interfaces observed using ultrafast coherent soft x-ray beams, Nat. Mater. 9 (2010) 26–30.
[243] H. Zhang, C. Hua, D. Ding, A.J. Minnich, Length dependent thermal conductivity measurements yield phonon mean free path spectra in nanostructures, Sci. Rep. 5 (2015) 9121.

[244] K.M. Hoogeboom-Pot, J.N. Hernandez-Charpak, X. Gu, T.D. Frazer, E.H. Anderson, W. Chao, R.W. Falcone, R. Yang, M.M. Murnane, H.C. Kapteyn, D. Nardi, A new regime of nanoscale thermal transport: collective diffusion increases dissipation efficiency, Proc. Natl. Acad. Sci. 112 (2015) 4846–4851.
[245] J. Cuffe, J.K. Eliason, A.A. Maznev, K.C. Collins, J.A. Johnson, A. Shchepetov, M. Prunnila, J. Ahopelto, C.M.S. Torres, G. Chen, K.A. Nelson, Reconstructing phonon mean-free-path contributions to thermal conductivity using nanoscale membranes, Phys. Rev. B 91 (2015) 245423.
[246] A.J. Minnich, Determining phonon mean free paths from observations of quasiballistic thermal transport, Phys. Rev. Lett. 109 (2012) 205901.
[247] L. Lindsay, First principles Peierls-Boltzmann phonon thermal transport: a topical review, Nanoscale Microscale Thermophys. Eng. 20 (2016) 67.
[248] L. Chaput, Direct solution to the linearized phonon Boltzmann equation, Phys. Rev. Lett. 110 (2013) 265506.
[249] C.D. Landon, N.G. Hadjiconstantinou, Deviational simulation of phonon transport in graphene ribbons with ab initio scattering, J. Appl. Phys. 116 (2014) 163502.
[250] P.B. Allen, J.L. Feldman, Thermal conductivity of disordered harmonic solids, Phys. Rev. B 48 (1993) 12581.
[251] P.B. Allen, J.L. Feldman, J. Fabian, F. Wooten, Diffusons, locons and propagons: character of atomic vibrations in amorphous Si, Phil. Mag. B 79 (1999) 1715.
[252] H.R. Seyf, A. Henry, A method for distinguishing between propagons, diffusions, and locons, J. Appl. Phys. 120 (2016) 025101.
[253] X. Chen, A. Weathers, J. Carrete, S. Mukhopadhyay, O. Delaire, D.A. Stewart, N. Mingo, S.N. Girard, J. Ma, D.L. Abernathy, J. Yan, R. Sheshka, D.P. Sellan, F. Meng, S. Jin, J. Zhou, L. Shi, Twisting phonons in complex crystal with quasi-one-dimensional substructures, Nat. Commun. 6 (2015) 6723.
[254] R.A. Guyer, J.A. Krumhansl, Thermal conductivity, second sound, and phonon hydrodynamic phenomena in nonmetallic crystals, Phys. Rev. 148 (1966) 778.
[255] R.A. Guyer, J.A. Krumhansl, Solution of the linearized phonon Boltzmann equation, Phys. Rev. 148 (1966) 766.
[256] J.A. Sussmann, A. Thellung, Thermal conductivity of perfect dielectric crystals in the absence of Umklapp processes, Proc. Phys. Soc. 81 (1963) 1122.
[257] R. Gurzhi, Thermal conductivity of dielectrics and ferrodielectrics at low temperatures, J. Exp. Theor. Phys. 46 (1964) 719–724.
[258] L. Mezhov-Deglin, Measurement of the thermal conductivity of crystalline He^4, J. Exp. Theor. Phys. 49 (1965) 66–79.
[259] V. Narayanamurti, R.C. Dynes, Observation of second sound in Bismuth, Phys. Rev. Lett. 28 (1972) 1461.
[260] H.E. Jackson, C.T. Walker, Thermal conductivity, second sound, and phonon-phonon interactions in NaF, Phys. Rev. B 3 (1971) 1428.
[261] C.C. Ackerman, W.C. Overton, Second sound in solid helium-3, Phys. Rev. Lett. 22 (1969) 764.
[262] S. Lee, L. Lindsay, Hydrodynamic phonon drift and second sound in a (20,20) single-wall carbon nanotube, Phys. Rev. B 95 (2017) 184304.
[263] Z. Ding, J. Zhou, B. Song, V. Chiloyan, M. Li, T.-H. Liu, G. Chen, Phonon hydrodynamic heat conduction and Knudsen minimum in graphite, Nano Lett. 18 (2018) 638–649.
[264] X. Li, S. Lee, Role of hydrodynamic viscosity on phonon transport in suspended graphene, Phys. Rev. B 97 (2018) 094309.
[265] A. Cepellotti, N. Marzari, Thermal transport in crystals as a kinetic theory of relaxons, Phys. Rev. X 6 (2016) 041013.
[266] J.-P.M. Péraud, N.G. Hadjiconstantinou, Efficient simulation of multidimensional phonon transport using energy-based variance-reduced Monte Carlo formulations, Phys. Rev. B 84 (2011) 205331.
[267] Q. Hao, G. Chen, M.-S. Jeng, Frequency-dependent Monte Carlo simulations of phonon transport in two-dimensional porous silicon with aligned pores, J. Appl. Phys. 106 (2009) 114321.
[268] X. Li, S. Lee, Crossover of Ballistic, Hydrodynamic, and Diffusive Phonon Transport, 2018 arXiv:1811.04329.
[269] N. de Koker, Thermal conductivity of MgO periclase from equilibrium first principles molecular dynamics, Phys. Rev. Lett. 103 (2009) 125902.
[270] T.M. Gibbons, S.K. Estreicher, Impact of impurities on the thermal conductivity of semiconductor nanostructures: first-principles theory, Phys. Rev. Lett. 102 (2009) 255502.
[271] H. Kim, S. Ballikaya, H. Chi, J.-P. Ahn, K. Ahn, C. Uher, M. Kaviany, Ultralow thermal conductivity of β-Cu_2Se by atomic fluidity and structure distortion, Acta Mater. 86 (2015) 247–253.
[272] J. Tersoff, New empirical model for the structural properties of silicon, Phys. Rev. Lett. 56 (1986) 632.
[273] B. Qiu, X. Ruan, Molecular dynamics simulations of lattice thermal conductivity of bismuth telluride using two-body interatomic potentials, Phys. Rev. B 80 (2009) 165203.
[274] L. Lindsay, D.A. Broido, Optimized Tersoff and Brenner empirical potential parameters for lattice dynamics and phonon thermal transport in carbon nanotubes and graphene, Phys. Rev. B 81 (2010) 205441.
[275] A. Rohskopf, H.R. Seyf, K. Gordiz, T. Tadano, A. Henry, Empirical interatomic potentials optimized for phonon properties, npj Comp. Mat. 3 (2017) 27.